ORIGINAL RESEARCH

Phosphonate-Modified Cellulose Nanocrystals Potentiate the Th1 Polarising Capacity of Monocyte-Derived Dendritic Cells via GABA-B Receptor

Marina Bekić [ID][1], Miloš Vasiljević [ID][2], Dušica Stojanović [ID][3], Vanja Kokol [ID][4], Dušan Mihajlović[2], Dragana Vučević[2], Petar Uskoković[3], Miodrag Čolić[1,2,5], Sergej Tomić [ID][1]

[1]Department for Immunology and Immunoparasitology, Institute for the Application of Nuclear Energy, University of Belgrade, Belgrade, Serbia; [2]Center for Biomedical Sciences, Medical Faculty Foča, University of East Sarajevo, Foča, Bosnia and Herzegovina; [3]Department for Construction and Special Materials, Faculty for Technology and Metallurgy, University in Belgrade, Belgrade, Serbia; [4]Department of Textile Materials and Design, Faculty of Mechanical Engineering, University of Maribor, Maribor, Slovenia; [5]Serbian Academy of Sciences and Arts, Belgrade, Serbia

Correspondence: Sergej Tomić, Institute for the Application of Nuclear Energy, University of Belgrade, Banatska 31b, Belgrade, Zemun, 11080, Serbia, Tel +381 11 2610 126, Fax +381 11 2618 724, Email sergej.tomic@inep.co.rs

Purpose: Phosphonates, like 3-AminoPropylphosphonic Acid (ApA), possess a great potential for the therapy of bone tumours, and their delivery via cellulose nanocrystals (CNCs) seems a promising approach for their increased efficacy in target tissues. However, the immunological effects of CNC-phosphonates have not been investigated thoroughly. The main aim was to examine how the modification of CNCs with phosphonate affects their immunomodulatory properties in human cells.

Methods: Wood-based native (n) CNCs were modified via oxidation (ox-CNCs) and subsequent conjugation with ApA (ApA-CNCs). CNCs were characterised by atomic force microscopy (AFM) and nanoindentation. Cytotoxicity and immunomodulatory potential of CNCs were investigated in cultures of human peripheral blood mononuclear cells (PBMCs) and monocyte-derived dendritic cells (MoDCs)/T cells co-cultures by monitoring phenotype, cytokines production, allostimulatory and Th/Treg polarisation capacity.

Results: AFM showed an increase in CNCs' thickens, elasticity modulus and hardness during the modification with ApA. When applied at non-toxic doses, nCNCs showed a tolerogenic potential upon internalisation by MoDCs, as judged by their increased capacity to up-regulate tolerogenic markers and induce regulatory T cells (Treg), especially when present during the differentiation of MoDCs. In contrast, ox- and ApA-CNCs induced oxidative stress and autophagy in MoDCs, which correlated with their stimulatory effect on the maturation of MoDCs, but also inhibition of MoDCs differentiation. ApA-CNC-treated MoDCs displayed the highest allostimulatory and Th1/CTL polarising activity in co-cultures with T cells. These effects of ApA-CNCs were mediated via GABA-B receptor-induced lowering of cAMP levels in MoDCs, and they could be blocked by GABA-B receptor inhibitor. Moreover, the Th1 polarising and allostimulatory capacity of MoDCs differentiated with ApA-CNC were largely preserved upon the maturation of MoDCs, whereas nCNC- and ox-CNC-differentiated MoDCs displayed an increased tolerogenic potential.

Conclusion: The delivery of ApA via CNCs induces potent DC-mediated Th1 polarisation, which could be beneficial in their potential application in tumour therapy.

Keywords: cellulose nanocrystals, phosphonates, dendritic cells, immunomodulation, GABA-B receptor

Introduction

Nanocellulose has become a highly attractive nanomaterial for various biomedical applications due to its excellent physico-chemical properties and a high potential for optimisation of its properties. Unlike cellulose nanofibers (CNFs) which contain large fibrils with alternating crystalline and amorphous structures, needle-like cellulose nanocrystals (CNCs) are much smaller and contain predominantly the crystalline part of nanocellulose.[1] Consequently, CNCs display high tensile strength and stiffness, high modulus of elasticity and high surface-to-volume ratio (Surface/Volume $\geq$3).[2] CNCs smaller than 200 nm in length are

generally considered biocompatible, making them suitable for tissue engineering and as drug delivery vehicles.[3–5] According to their capacity to accumulate in tumours via the Enhanced Permeability and Retention (EPR) effect, CNC showed great potential for tumour targeting.[6] Moreover, the preference to transiently migrate into bones makes CNCs excellent for the delivery of drugs in these hardly accessible tissues.[7] Bones are commonplace for colonisation and growth of metastatic tumours, such as breast cancer and prostate cancer, which subsequently cause spans to diffuse osteopenia, focal osteolysis, osteomalacia, etc.[8] In line with this, the delivery of anti-osteoporotic phosphonates and cytotoxic drugs via CNCs has been considered an attractive approach for the therapy of osteosarcoma and bone metastasis.[9,10] Namely, phosphonates, such as alendronate (ALN) and 3-aminopropyl phosphonic acid (ApA), were shown to inhibit osteoclast-mediated bone resorption and increase bone mineralisation.[11,12] Moreover, we showed previously that ALN and ApA conjugated to CNCs display good biocompatibility and the growth of primary human osteoblasts,[13] all of which could be desirable in treating bone diseases with prominent osteolysis. Besides preventing osteolysis, cancer therapy ought to induce an efficient systemic immune response capable of eliminating tumour cells. However, the immunological properties of CNCs, especially when conjugated with bisphosphonates, have not been investigated previously in this context.

The immune response is critically regulated by dendritic cells (DCs). They are the most effective antigen-presenting cells (APCs) capable of activating naïve T cells and regulating their differentiation into effector populations of T helper (Th) 1, Th17 cells, and cytotoxic CD8+ T lymphocytes (CTL), all of which are critically involved in the elimination of tumour cells.[14] The features of DCs that can trigger an efficient anti-tumour response include phenotypically mature DCs, expressing highly human leukocyte antigen (HLA)-DR, CD83, costimulatory molecules (ie CD80, CD86) and producing high levels of interleukin (IL)-12 that is necessary for the induction of Th1/CTLs.[15,16] The delivery of stimulatory molecules for DCs via nanoparticles is a highly attractive approach in tumour therapy, which can increase the efficacy of DCs stimulation and reduce potential adverse effects of drugs in a soluble form, as we showed previously with carbon nanotubes conjugated with a toll-like receptor (TLR)-7 agonist.[17] However, the stimulation of DCs precursors during their differentiation can promote their semi-mature and tolerogenic properties, as we demonstrated previously,[18] and pathogens utilise this strategy to bypass DC-mediated induction of adaptive immune response.[19] Semi-matured and tolerogenic DCs display elevated expression of tolerogenic molecules such as Immunoglobulin-Like Transcript (ILT) 3, ILT4, Programmed Death-Ligand (PD-L) 1, Indoleamine 2,3-Dioxygenase (IDO)-1, and produce regulatory cytokines such as IL-10, IL-27 and Transforming Growth Factor (TGF)-β.[20,21] These properties correlate with a high capacity of DCs to induce Th2 and T regulatory cells (Tregs), which are highly adverse in tumour therapy since they support tumour growth and metastasis.[22–24]

Previously, we showed that native CNFs induce tolerogenic properties in monocyte-derived (Mo) DCs, which display a high capacity to induce Th2 cells and CD4+CD25hiFoxP3+ Tregs.[25] This capacity of CNF was additionally potentiated when CNFs were oxidised and functionalised with ApA,[26] indicating that CNF nanoplatforms could be harnessed for the therapy of inflammatory T cell-mediated pathologies, but could be highly adverse in tumour therapy. Due to different physicochemical properties, CNC could induce quite different immunological effects.[3] Most studies explored the immunological effects of CNC in the context of respiratory toxicity.[3,27,28] It was shown that the exposure of macrophages to CNC potentiates their polarization towards the M1 phenotype and increases the production of proinflammatory cytokines.[29] In addition, mouse bone marrow-derived DCs treated with native CNC showed increased expression of MHC II, CD86 and CD40, followed by NLRP3 inflammasome-driven IL-1β secretion.[30] These pro-inflammatory effects of CNC were observed as a part of their immunotoxic or subtoxic effects, such as lysosomal damage and induction of ROS. However, it remained utterly unknown whether any tolerogenic effects could be induced by non-toxic doses of CNC. Additionally, the functional changes induced by CNC on APC were poorly investigated, especially on how the treated APC interact with T cells. Therefore, the primary major aim of this study was to investigate the effects of native, oxidized and ApA-modified CNC in different models of human APC-T cell interactions in vitro. We found that nCNC display anti-inflammatory and pro-tolerogenic properties in human immune cells, whereas the oxidation and ApA conjugation diminish those properties. The conjugation of ApA to CNC was found to potentiate MoDCs capacity to induce Th1 polarization via GABA-B receptor-mediated down-regulation of cAMP levels, all of which could be beneficial for their potential application in tumour therapy.

Materials and Methods

Synthesis and Characterization of Cellulose Nanocrystals

Native CNCs, 150–200 nm long (4 wt.% dispersion in Milly-Q), were derived from raw wood pulp, and they were prepared by sulfuric acid hydrolysis. Native CNCs were then oxidised and conjugated with ApA as described previously.[13] Briefly, nCNCs were oxidised by dissolving 1.6 g of sodium periodate (NaIO$_4$) in 50 mL of Milly-Q water and adding to 50 mL of 4 wt.% nCNC dispersion. Homogenous dispersion was obtained by mixing and shaking in an additional 100 mL of Milly-Q water, for the next 24 h at room temperature. After that, the dispersion was dialysed against Milly-Q water for 48 h. The remaining CNC dispersion containing oxidized CNC (ox-CNCs) was washed additionally with 0.1 M of acetate buffer (pH 4.5) and stored at 4 °C for further conjugation and usage. For ApA conjugation on ox-CNC, 0.45 g of ApA (Sigma Aldrich, St. Louis, Missouri, USA) was dissolved in 1.5 mL of 0.1 M acetate buffer (pH 4.5) and 0.5 mL of ApA-containing solution was added to 100 mL of ox-CNC. ApA-CNCs were washed separately in Milly-Q water until the total removal of unreacted ApA. The stock solutions of nCNCs (11.8 wt.%), ox-CNCs and ApA-CNCs (both 4.25 wt.%), were stored at +4 °C prior to use in biological assays. The final extent of conjugated ApA to oxCNCs was 7 wt.%, as determined by spectroscopic analysis and FTIR.[13]

Detailed characterisation of nCNC, ox-CNC and ApA-CNC by ATR-FTIR, UV-Vis spectroscopy, Dynamic Light scattering (DLS), Nanoparticle Tracking Analysis (NTA) and Transmission Electron Microscopy (TEM) was reported previously.[13] Here, we additionally analysed the surface morphology by atomic force microscopy (AFM) with NanoScope 3D (Veeco, Oyster Bay, New York, USA) microscope operated in tapping mode under ambient conditions. Etched silicon probes with a spring constant of 20–80 Nm^{-1} were used. Image analysis was done using the Nanoscope image processing software. Before morphological examinations, the mica substrate was mechanically polished with adhesive tape, and 10 μL of prepared suspension of nCNC, ox-CNC or ApA-CNC were deposited on a polished mica substrate and dried on air for 24 h before the analysis.

Nanoindentation experiments were carried out using a Triboscope T950 Nanomechanical Testing System (Hysitron, Minneapolis, MN, USA) equipped with a Berkovich tip indenter and scanning probe microscopy, at a room temperature of 20 °C and relative humidity of up to 30%. The load and the depth penetration were recorded continuously throughout the loading-unloading cycles. Based on the proposed method,[31] the extrapolation of a tangent to the top of the unloading curve was used to determine the depth (a combination of elastic and plastic displacement) over which the indenter is in contact with the specimen at the maximum load, Pmax. Indentation hardness was defined as applied load per unit area of indentation. For a maximum load P_{max}, the hardness H was calculated as:

$$H = \frac{P_{max}}{A} \tag{1}$$

where A is the projected contact area between the indenter and the sample surface.

The slope of the unloading curve provided a measure of the contact stiffness, which was used with the contact area to determine the elastic modulus. The elastic (reduced) modulus (E_r) obtained is related to the material properties of the specimen and the indenter, and the relationship between the stiffness and reduced modulus is:

$$S = \frac{2E_r\beta\sqrt{A}}{\sqrt{\pi}} \tag{2}$$

Where S is the contact stiffness of the material, and constant β=1.034 for a Berkovich indenter. The relationship between indentation modulus, E, and the reduced modulus, E_r, of the sample is given by:

$$\frac{1}{E_r} = \frac{\left(1-\nu^2\right)}{E} + \frac{\left(1-\nu_i^2\right)}{E_i} \tag{3}$$

Where E and v are the elastic modulus and the Poisson's ratio ascribed to the CNC samples, respectively, whereas E_i and v_i are the same parameters for the indenter.[32] In this work, v was set as 0.45, E_i and v_i are equal to 1140 GPa and 0.07 for Berkovich diamond tips, respectively. The indentation maximum load was set to 250 μN with the load-hold-unload of

5-2-5s for each segment; at least nine indents were performed at different points on the surface and the average values and standard deviations are reported.[33]

Cells

Cytocompatibility and immunomodulatory properties of CNCs were tested in vitro using human peripheral blood mononuclear cells (PBMCs) and MoDCs. Before human blood sample collection, written informed consents were provided by health donors, in accordance with the Declaration of Helsinki and approvals by the Ethical Committee of the Institute for the Application of Nuclear Energy (INEP). PBMCs were isolated from buffy coats by density gradient centrifugation in LymphoprepTM gradient media (Axis Shield PoC AS, Oslo, Norway), according to the manufacturer's instructions. Monocytes and T cells were purified from PBMCs by magnetic-activated cell sorting (MACS) using Monocyte Isolation Kit and Pan T cell Isolation Kit (all Miltenyi Biotec, Bergisch Gladbach, Germany), where LS column flow-through represented the enriched populations of CD14$^+$ monocytes and CD3$^+$ T cells, respectively.

Experimental Treatments

Freshly isolated PBMCs (4×10^5/well of the 96-wells plate in 4-plicates) were cultivated in a complete RPMI-1640 medium containing 10% foetal calf serum (FCS), 50 µM 2-mercaptoethanol (all from Sigma-Aldrich, St. Louis, Missouri, USA), and antibiotics (100 U/mL penicillin, 20 µg/mL gentamicin, 100 U/mL streptomycin (Galenika, Belgrade, Serbia)) in the presence of nCNCs, ox-CNCs or ApA-CNCs in serial dilutions (50, 100, 200, 400, 800 µg/mL). The cells were cultivated for 24 h or 48 h at 37°C, 5% CO$_2$ and 90% humidity, followed by the analysis of metabolic activity, cell death, proliferation, and cytokine production.

Immature MoDCs were generated by cultivating MACS-purified monocytes (2×10^6 cells in 6-well plates) in CellGenix® GMP Dendritic Cell Medium (CellGenix, Freiburg im Breisgau, Germany) in the presence of human recombinant GM-CSF (20 ng/mL, Novus Biologicals, Toronto, Canada) and human recombinant IL-4 (20 ng/mL, Roche Diagnostics, Basel, Switzerland) for 4 days. To induce the maturation of MoDCs, the cells were stimulated on day 4 with lipopolysaccharide (LPS) from Escherichia coli serotype *0.111:B4* (200 ng/mL; Sigma-Aldrich, activity: 5 EU/ng (Limulus Amoebocyte Lysate test)) and human recombinant interferon (IFN)-γ (20 ng/mL, R&D Systems, Minneapolis, MN, United States) for next 16–18 hours, whereas corresponding immature MoDCs were left unstimulated. To assess the effects of CNCs on the differentiation of MoDCs, monocytes were treated with nCNCs, ox-CNCs or ApA-CNCs (200 µg/mL) for 4 days, followed by LPS/IFN-γ treatment for the next 16 h. The effect on MoDCs maturation was investigated by differentiating immature MoDCs without CNCs for 4 days, and then treating them with nCNCs, ox-CNCs or ApA-CNCs (all at 200 µg/mL) for 3 hours before the induction of maturation with LPS/IFN-γ, as described. Besides CNC samples, additional control groups in those experiments were MoDCs treated with soluble ApA at a dose equivalent to that attached to ApA-CNCs (14 µg/mL, corresponding to 7 wt.% of ApA in ApA-CNCs, sApA1x), and MoDCs treated with 5 times higher dose of soluble ApA (70 µg/mL, sApA5x). After the cultures where MoDCs were harvested, their number and viability were determined using Trypan-blue viability dye and Annexin V/7- amino-actinomycin D (7-AAD) staining, respectively. The phenotype of MoDCs was analysed by microscopy and flow cytometry (LSR II, Beckton Dickenson, California, United States), whereas the functions of these cells were further analysed in co-cultures with MACS-purified allogeneic T cells. Cell-free supernatants were collected and stored at −20 °C to detect cytokine levels.

Cytotoxicity Assays, Autophagy and ROS Production

The metabolic activity of PBMCs in cultures with CNC was performed by using an MTT assay. MTT (3-(4,5-dimethylthiazol-2-yl)-2,5-diphenyltetrazolium bromide) was added after the cultures at the final concentration of 0.5 mg/mL to each well for 4 h. Cell-free cultures with corresponding concentrations of CNC were used as blank controls. Formazan crystals that were formed were dissolved by overnight incubation of samples in 10% (w/v) sodium dodecyl sulphate (SDS, Millipore, Burlington, Massachusetts, United States) and 0.01N (v/v) hydrochloric acid (HCl, Sigma-Aldrich). Finally, the absorbance was measured on a microplate reader at 570nm (ELx800, Biotek, Winooski, Vermont, United States), and the reference wavelength was 670 nm (the corrected OD=OD570-OD670 for each well).

The relative metabolic activity (MTT %) in culture was calculated by subtracting the corrected OD value from the corresponding blank controls and normalising the results to control non-treated PBMCs (100%).

To determine the mode of cell death in PBMCs/CNC cultures, the cells were harvested after 48 h, and necrosis and apoptosis were determined after staining of non-permeabilized and permeabilised cells, respectively, with PI (50 μg/mL, Sigma-Aldrich). Namely, total dead cells (predominantly necrotic cells) were identified as PI^+ cells by flow cytometry. The percentage of apoptotic cells was determined by analysing sub-G1 peak in the cells that were fixed/permeabilised with ice-cold 75% ethanol added dropwise while vortexing the cell pellet and then stored for 2 h at −20 °C, followed by PI staining in PBS.

The cytotoxicity of CNC samples in MoDCs cultures was determined by Annexin-V/7-AAD staining using Muse Annexin V & Dead Cell Reagent Kit (Luminex Corporation, Texas, United States), according to the manufacturer's instructions. The autophagy flux was analysed in MoDCs after the cultures using Muse Autophagy Kit (Luminex), which is based on the detection of a membrane-converted variant of LC3-II. The MoDCs were either stained directly or washed first in PBS and then incubated for 4 h in PBS (starving conditions) in the presence of Bafilomycin according to the manufacturer's protocol. For the detection of reactive oxygen species (ROS), we used Muse Oxidative Stress Kit (Luminex), which is based on the staining of cells with dihydroethidium (DHE). The analysis of apoptosis, autophagy and oxidative stress was performed on Guava Muse Cell Analyzer (Luminex).

Mixed Leukocyte Reaction

To assess the endotoxin levels in the CNC samples, PBMCs were treated with CNC samples (400 μg/mL), 0.1, 1, 10 or 100 ng/mL of LPS, either with or without the polymyxin B (10 μM, Sigma-Aldrich, PxB) for 24 h, followed by the measurements of IL-1β levels in supernatants. The proliferation and cytokine production by PBMCs were determined in phytohemagglutinin (PHA, 20 μg/mL, Sigma-Aldrich)-stimulated PBMCs cultivated with CNC (50, 100, 200, 400, 800 μg/mL) for 4 days and 48 h, respectively. To assess the proliferation, PBMCs were first labelled the cells with CellTrace Far Red dye (Invitrogen, Massachusetts, United States), according to the manufacturer's protocol, followed by 4 days of cultivation in a complete RPMI medium. After that, the cells were harvested, filtered through 30 μm pore filters, and stained with PI (50 μg/mL, Sigma Aldrich). CellTrace Far Red dye dilution was analysed after excluding doublets and PI^+ cells by flow cytometry.

To assess the functions of CNC-treated MoDCs, allogeneic MLR were performed, in which allogeneic purified T cells were used as responders. To analyse the capacity of MoDCs to stimulate T cell proliferation, MoDCs ($1x10^4 – 0.25x10^4$/ well of the round-bottom 96-wells plate) were co-cultivated with allogeneic T cells ($1x10^5$/well) pre-labelled with CellTrace Far Red dye (Invitrogen), thus providing 1:10 −1:40 MoDC: T cell ratios, respectively. MoDCs were co-cultivated with T cells for 4 days, and CellTrace Far Red dilution was determined by flow cytometry, as described for PBMCs. To monitor the T cell polarisation capacity of MoDCs, MoDCs/T cell cultures were treated with Phorbol 12-myristate 13-acetate (PMA, 20 ng/mL) and ionomycin (500 ng/mL) (both from Sigma-Aldrich) for the last 6 h before harvesting the cell-free supernatants for cytokines measurements. To detect intracellular cytokines in T cells, the co-cultures were treated with PMA/ionomycin and monensin (2 μM, Sigma-Aldrich) for the last 4 h of incubation, then stained with specific antibodies and analysed by a flow cytometer.

Microscopy Analyses

Single-cell suspensions were prepared after 48h-cultures of PBMCs or 24h-cultures of MoDCs with CNC samples, and the cytospins were prepared ($1x10^4$ cells/70μL PBS) by using Rotafix 32 Centrifuge (Andreas Hettich GmbH & Co., Tuttlingen, Germany) and air-dried. The samples were prepared for epi-fluorescent microscopy (AxioImager A1, Carl Zeiss), by staining the cells with anti-HLA-DR-Alexa Fluor 488 (1:100 dilution, BioLegend, San Diego, California, United States), Calcofluor White stain (1:100 dilution, Sigma-Aldrich) and PI (5 μg/mL), in a humidity chamber for 30 min. After rinsing in PBS, the samples were mounted with Mounting Media (Thermo Fisher Scientific, Waltham, Massachusetts, USA) and monitored with a UV filter set for Calcofluor White (UV-2B, ex: 330–380 nm, DM 400, BA 435), green filter set for detection of anti-HLA-DR-Alexa fluor 488 (B-2A, ex: 450–490 nm, DM 505, BA 520) and red filter set for detection of PI (G-2A, ex: 510–560 nm, DM 575, BA 590). The images taken by each filter set were

acquired as monochromatic and later merged offline in ImageJ software (National Institutes of Health, Bethesda, Maryland, USA). Semiquantitative analysis of CNC internalisation was performed by counting the cells, which did not internalise CNC (score 0), those which internalised CNC partially (score 1), or those which completely internalised CNC, as judged by enclosed membrane around the CNCs (score 2). At least 300 cells/slide were scored from two independent experiments, and two different observers performed the scoring. Additionally, the internalisation of CNCs was analysed by monitoring the side scatter (SSC) and forward scatter (FSC) parameters on the flow cytometer, as indicators of DCs' granularity and size, respectively, both of which vary depending on the nanoparticles' internalisation and their interaction with the cell surface.[17,26,34]

Flow Cytometry Analysis

The phenotypes of MoDCs and T cells after the cultures were analysed by flow cytometry. The cells were washed once in PBS containing 2% FCS and 0.01% Na-azide (Sigma-Aldrich), treated with Human TruStain FcX (BioLegend) for 15 minutes, and then labelled with fluorochrome-labelled monoclonal antibodies. The following antibodies were used for labelling at dilutions recommended by the manufacturer: IgG1 negative control-phycoerythrin (PE) (MCA928PE), IgG1 negative control-fluorescein isothiocyanate (FITC) (MCA928F) (Bio-Rad Laboratories, Hercules, California, United States); anti-CD1a- Peridinin-Chlorophyll-Protein (PerCP)/Cyanine (Cy) 5.5 (HI149), anti-HLA-DR-Allophycocyanin (APC)/Cy7 (L234), anti-IL-4-PerCP/Cy5.5 (MP4-25D2), anti-IL-4-PE (MP4-25D2), anti-ILT-4-APC (42D1), anti-CD25-PE (BC96), anti-CD25-PerCP/Cy5.5 (M-A251), anti-CD127-PE (A019D5), anti-IL-10-APC, anti-IL-10-PE (JES5-16E3), anti-TGF-β-APC (TW4-6H10), anti-IL17A-Alexa Fluor 488 (BL168), anti-IFN-γ-APC, anti-IFN-γ-FITC (4S.B3), anti-CD83-FITC (HB15e), IgG1 negative control-PerCP/Cy5.5 (HTK888), anti-PD1L-PE (29E.2A3), anti-IL-33-biotin (poly5163) (all from BioLegend); anti-HLA-DR-PerCP (L243), anti-IDO-1-APC (700838), anti-CD4-FITC, anti-CD4-APC (11830), anti-TGF-β-PE (9016) (all from R&D Systems, Minnesota, United States), anti-CD14-FITC (TUK4), anti-NLRP3-APC (rea668), anti-IL-1β-PE (rea1172) (all from Miltenyi Biotec); anti-CD86-PE (IT2.2), streptavidin-PerCP, streptavidin APC, anti-ILT3-PE (ZM4.1), anti-CD209-FITC (eBh209), IgG1 negative control APC (MA5-18093), anti-IL-17A-APC (eBio17B7) (all from Thermo Fisher Scientific); anti CD40-APC (5C3), anti-IL-12 (p40/p70)-PE (C11.5), anti-CD3-PE (SK7), anti-FoxP3-PerCP/Cy5.5, anti-FoxP3-Alexa Fluor 488 (236A/E7), anti-RORγt-Alexa Fluor 488 (Q21-559), anti-GATA-3-Alexa Fluor 488 (L50-823) (all from BD Biosciences, San Diego, California, United States), anti-CD8-PerCP/Cy5.5 (HIT8a) (Elabscience, Texas, United States).

The incubation lasted for 30 min at 4 °C. Intracellular staining was carried out after the surface labelling with the fixation and permeabilization kit (BioLegend). For each analysis, doublets were excluded according to forward scatter (FSC)-A/FSC-H, and more than 5000 cells were gated according to their specific FSC-A/side-scatter (SSC)-A properties, thereby avoiding the cells with low FSC-A/SSC-A properties, representing predominantly dead cells. Signal overlap between the channels was compensated before each experiment by using single fluorescence labelled cells, and the non-specific fluorescence was determined by using appropriate isotype control antibodies and fluorescence minus one (FMO) controls. The samples were acquired on an LSR II flow cytometer (BD Biosciences) on the day of sampling and analysed offline in FCS Express 4 software (De Novo software, California, United States) and FlowJo vX (BD Biosciences).

Quantitative Polymerase Chain Reaction

Total RNA was extracted from MACS sorted CD14$^+$ monocytes from two donors (day 0), and every day during their differentiation with GM-CSF/IL-4 into immature MoDCs (from day 1 to day 4). The cells were harvested, and total RNA was extracted using the Total RNA Purification Mini Spin Kit (Genaxxon Bioscience GmbH, Ulm, Germany) according to the manufacturer's instructions. The cDNA was reverse-transcribed from 50 ng of total isolated RNA using a High-Capacity cDNA Reverse Transcription Kit (Thermo Fisher Scientific). Synthesised cDNA was amplified in a 7500 real-time PCR system (Applied Biosystems, Massachusetts, United States) using a SYBR Green PCR Master Mix (Thermo Fisher Scientific). Amplification was performed by denaturation at 95 °C for 10 min, followed by 40 cycles of 95 °C for 30 sec, 58 °C for 30 sec and 72 °C for 30 sec. PCR primers used here were as follows. β-actin: 5′- TCAGTAACAGTCCGCCTAGAAGCA −3′ (sense), 5′-TGCTGACAGGATGCAGAAGGAGA −3′ (antisense); GABA-B R1 subunit: 5′-TGGCATGGACGCTTATCGA-3′ (sense), 5′-GATCATCCTTGGTGCTGTCATAGT-3′ (antisense); GABA-B R2 subunit: 5′-CTGGTATTCGTGCCGAAGCT-3′ (sense), 5′-TGAACTGGAATCGCCTGTTCT-3′ (antisense). All primers were designed

with Primer Express v.3.0.1 (Applied Biosystems) and purchased from Thermo Fisher Scientific. β-actin was performed on each experimental setup as an endogenous control. The results were normalised against the β-actin gene and expressed as relative target abundance using the $2^{-\Delta\Delta Ct}$ method. All reactions were run in triplicates.

cAMP Measurement

To determine the role of GABA-B Receptor and cAMP signalling, immature MoDCs ($2x10^5$ cells/96 well plate) were seeded in CellGenix® GMP Dendritic Cell Medium and treated with Baclofen (30 µM Sigma-Aldrich), ApA (14 µg/mL or 70 µg/mL), ApA-CNC (200 µg/mL) either in the presence or absence of GABA-B receptor blocking agent CGP52432 (10 µM, Tocris Bioscience, Bristol, United Kingdom) for 10 minutes. CGP52432 was added to MoDCs cultures 30 min before the treatments. Similar experiments were performed in MoDCs stimulated with 10 µM Forskolin (Sigma-Aldrich). Based on enclosed instructions, intracellular cAMP levels were determined using cAMP competitive ELISA kit (Invitrogen). MoDCs were washed and lysed with 0.1% (w/v) Triton X-100 (Millipore Sigma) in 0.1M (v/v) HCl for 10 minutes at room temperature. After centrifugation, cell- and debris-free supernatants were stored frozen for later analysis. The acetylated version of the assay was performed, by acetylating samples and standards with Acetylating Reagent in the Kit. The absorbance was measured at a microplate reader at 405nm with correction at 630nm (ELx800, BioTek). Total protein content was measured using a Pierce™ BCA protein assay Kit (Thermo Fisher Scientific). BSA standard or samples were transferred to a 96-well plate to which working reagents were added (working reagent 50:1 ratio of assay reagents A and B). The plate was incubated for 30 min at 37 °C, before reading the absorbance at 570nm at the microplate reader (ELx800, BioTek). To normalise the level of cAMP for protein content, the resulting pmol/mL was divided by the total protein concentration (mg/mL) in each sample. The results are expressed as cAMP in pmol/mg of total protein.

Cytokine Measurement

Supernatants from PHA-stimulated PBMCs cultures were collected after 48 h and assayed for cytokine measurements using LEGENDplex™ Human Inflammation Panel 1 (BioLegend). DC cultures were assayed for IL-12p17, IL-23, IL-10 and IL-1β, whereas DC/T cell co-cultures were analysed for IL-5, IL-10, IL-17 and IFN-γ by specific sandwich enzyme-linked immunosorbent assay (ELISA) (all from R&D Systems).

Statistical Analysis

To analyse the differences between treatment and control groups, a repeated-measures one-way analysis of variance (RM-ANOVA) was performed, followed by Tukey's multiple comparison test (GraphPad Prism 8). Data are presented as means ± SD of the indicated number of independent experiments, and a p-value of <0.05 was considered to be a significant difference between the groups.

Results
Oxidation and ApA-Modification Increase the Elasticity and Hardness of CNCs

First, ox-CNCs were prepared from nCNCs by periodate oxidation, which cleavaged the C2-C3 bond of the glucopyranose ring, converting the respective vicinal hydroxyl into two aldehyde groups (Figure 1A). Ox-CNCs were then modified with ApA, using a Schiff-base coupling reaction between the amine groups of ApA and the aldehyde groups of ox-CNCs, as described previously.[13] ATR-FTIR vibrational bands confirmed the described formations of aldehyde groups in ox-CNCs, and their conversion into C-N bounds after the modification with ApA. Based on the FTIR spectra, as well as spectroscopic analysis, about 7 wt.% of ApA was attached to the surface of ox-CNCs in ApA-CNCs. The modifications described were followed by changes in CNCs' hydrodynamic sizes, z-potentials, nanoparticle tracker analysis (NTA) properties and TEM properties, as described previously.[13]

Nanoparticles' shape and size,[23,35] as well as their elasticity modules,[36] were found to be critical for the interaction with cells. Previous characterisation of CNCs[13] lacked a precise analysis of nanocrystal size, and it remained unknown how the elasticity modules of CNCs change after their oxidation and ApA modification. Therefore, we performed AFM and
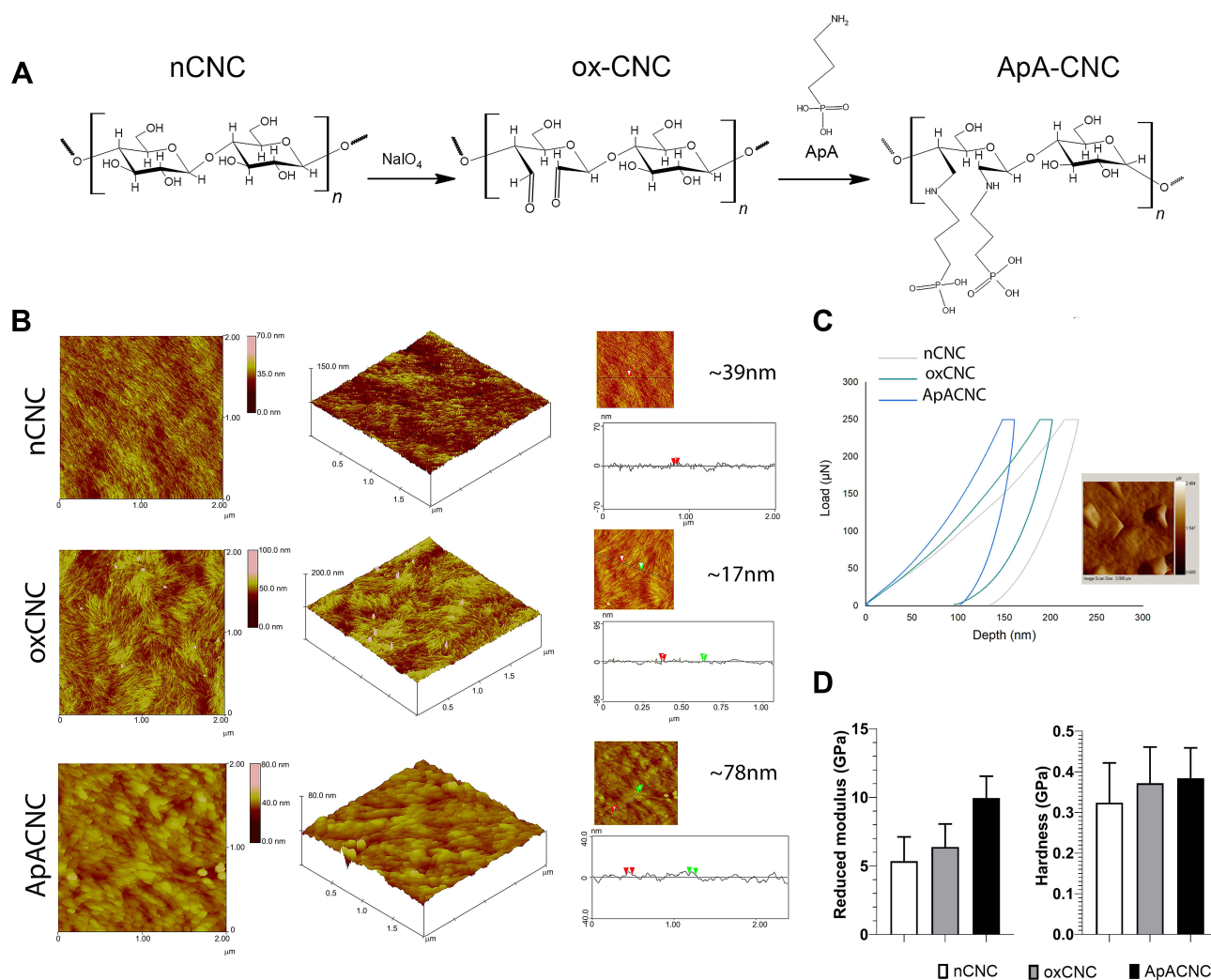
Figure 1 Characterization of native, oxidized and ApA-modified CNCs. (**A**) Chemical structures of CNCs used in the study. (**B**) AFM images of top-view analysis (scan size of 2×2 μm) (left), surface area plot analysis (middle), and cross-section analysis with indicated nanocrystal thickness measurements (right, marked by red or green triangles) are shown. (**C**) Nanoindentation analysis for native and modified CNCs, and scanning probe microscope (SPM) image showed the indents at ApA-CNCs (scan size of 3×3 μm). (**D**) Summarized data for reduced elasticity and hardness is shown as mean ± SD of 9 randomly selected measurements on the same CNC preparation. Surface plot analysis.

nanoindentation analysis (Figure 1B–D) to assess the morphology and elasticity of nCNCs, ox-CNCs and ApA-CNCs during the modifications. AFM data showed significant changes in CNC morphology upon modifications. AFM showed that CNCs are tightly packed on the mica substrate, and the crystallinity of CNCs was clearly preserved. The average thickness of nCNCs was about 39 nm and the oxidation of nCNCs reduced the thickness to about 17 nm in oxCNCs. On the other hand, ApA modification increased the thickness of nanocrystals to about 78 nm, and the nanocrystals appeared amorphous compared to sharply define ox-CNCs (Figure 1B). Nanoindentation analysis (Figure 1C) showed an outstanding increase of reduced elastic modulus, from 5.35± 1.77 GPa to 9.95± 1.59 GPa, and from 0.324 ± 0.098 GPa to 0.384± 0.075 GPa for indentation hardness of CNC samples. Thereby, the reduced elasticity modules and hardness of CNCs increased after oxidation, and further, with ApA modification, as compared to nCNCs (Figure 1D).

Non-Cytotoxic Doses of CNCs Displayed Immunomodulatory Potential in Cultures with PBMCs

To assess the immunomodulatory potential of native and modified CNCs, we first determined their dose-dependent cytotoxicity (CNCs: 50–800 μg/mL) in cultures with human PBMCs to determine the non-toxic doses for the following

immunomodulation assessment. First, we performed an MTT assay and evaluated the cell death (apoptosis and necrosis) by flow cytometry (Figure 2A) after 24 h and 48 h cultures. All the CNC samples reduced MTT% significantly at 800 µg/mL, whereas the lower doses had no significant effects after 24 h (not shown) and 48 h cultures (Figure 2A). Since MTT measures both metabolic activity and cytotoxicity, we also analysed apoptosis and necrosis in PBMC. The measurements of PBMCs with hypodiploid nuclei (predominantly apoptotic) and permeabilised cells (predominantly necrotic) suggested that both apoptosis and necrosis were increased in PBMCs treated with 800 µg/mL CNC, as compared to control non-treated cells. At 400 µg/mL, nCNC displayed a slight increase in the % of apoptotic cells (<20% increase), which according to ISO 10993–5:2009 standard, can be considered as a non-toxic effect.

PBMC treated with CNC samples alone (400 µg/mL) did not produce significant levels of IL-1β after 24 h, unlike PBMC treated with 0.1 ng/mL or 1 ng/mL of LPS (1 ng/mL is equivalent to 5 EU/mL), which could be blocked with PxB (10µM) (data not shown), suggesting that the CNC samples at the tested doses had less than 0.5 U/mL of endotoxin present. The effects of CNC on the proliferation of CellTrace Far Red-loaded PBMCs induced by PHA, a potent polyclonal T-cell mitogen.[37] It was found that ApA-CNCs stimulate the proliferation of PHA-treated PBMCs at 200 µg/mL and 400 µg/mL, compared to control PHA-PBMCs. In contrast, nCNCs displayed an inhibitory effect on the PHA-induced proliferation in doses of 200, 400, and 800 µg/mL (Figure 2B). The doses of CNCs higher than 400 µg/mL were not further analysed due to their cytotoxic effects.
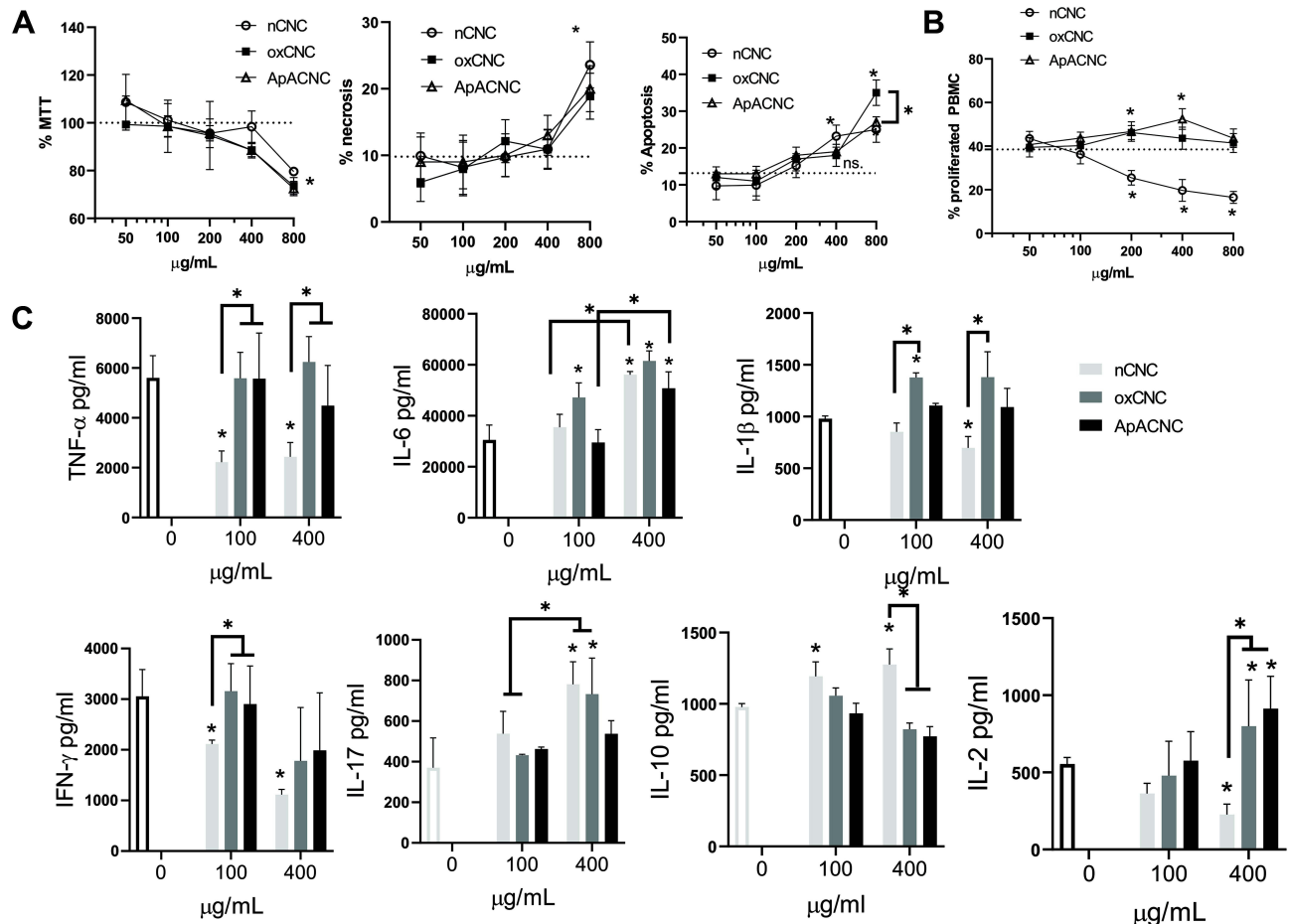

Figure 2 Dose-dependent cytotoxic and modulatory effects of CNC samples on PBMCs. (**A**) Relative metabolic activity (% MTT), % of necrotic and % of apoptotic cells were determined in 48h-cultures of PBMCs (3×10^5/well of 96 well-plate) and two-fold increasing concentrations of CNC (from 50 to 800 µg/mL). Data is presented as mean ± SD from 3 independent experiments, and a dotted line represents the mean value of control non-treated PBMCs. (**B**) The proliferation of PHA-stimulated PBMCs, cultivated in the presence of CNCs (from 50 to 800 µg/mL) was determined by CellTrace Far Red dilution assay and the values are shown as mean ± SD of three independent experiments. (**C**) Dose-dependent effects of CNCs on cytokine production by PHA-PBMCs after 48h cultures. The indicated cytokines were measured from cell-culture supernatants by ELISA and the results are shown as mean ± SD from three independent experiments. *p<0.05 vs control non-treated PBMC, or as indicated (RM-ANOVA, Tukey's multiple comparison test).

Besides proliferation, we evaluated the modulatory effects of CNCs in non-toxic (100 µg/mL) and subtoxic doses (400 µg/mL), on cytokine levels in 48 h PHA-PBMCs cultures (Figure 2C), by monitoring proinflammatory cytokines (TNF-α, IL-6, IL-1β), Th1 cytokines (IFN-γ, IL-2), Th17 (IL-17), Th2 (IL-4) and immunoregulatory cytokine (IL-10). It was found that nCNCs inhibited PHA-induced production of TNF-α and IFN-γ at both 100 µg/mL and 400 µg/mL, as well as IL-2 and IL-1β in the higher doses applied (400 µg/mL). Additionally, nCNCs stimulated the production of IL-6 and IL-17 at higher doses used, whereas IL-10 was induced by both lower and higher doses of nCNC-treated PHA-PBMCs. ApA-CNCs induced IL-2 and IL-6 in higher doses, without significantly affecting the levels of other cytokines, whereas ox-CNCs stimulated the production of IL-1β and IL-6 at lower doses, as well as IL-6, IL-17 and IL-2 in higher doses applied in PHA-PBMCs cultures. The levels of IL-4 in the examined PHA-PBMCs co-cultures were below the detection limit (data not shown). These results suggested that the lower doses of nCNCs induce predominantly anti-inflammatory properties in PHA-PBMCs cultures but potentiate IL-6 and IL-17 in subtoxic doses. In contrast, ApA- and ox-CNCs lacked the anti-inflammatory potential PHA-PBMCs in non-toxic doses, and ox-CNCs even potentiated the production of pro-inflammatory cytokines.

Internalisation, Induction of ROS and Autophagy in Dendritic Cells Depend on CNCs Modification

PHA-stimulated PBMCs are a standard model for screening the immunomodulatory effects of nanomaterials.[38] The stimulation of lymphocyte proliferation and cytokine production in this model depends on the presence of endogenous antigen-presenting cells (APCs) within PBMCs.[39,40] Additionally, the analysis of the interaction between PBMCs and nCNCs suggested that HLA-DR+ B lymphocytes, and HLA-DR- lymphocytes had no internalised nCNCs, unlike larger phagocytic cells, most probably monocytes/macrophages and DCs (Supplementary Figure 1). Therefore, we investigated the modulatory effects of CNCs on APCs in more detail by using human MoDCs as a model system. The dose of 200 µg/mL of each CNCs was chosen as the highest non-toxic dose which induces modulatory effects in PBMCs, but not cytotoxicity.

MACS-purified monocytes were differentiated into immature MoDCs in the presence of GM-CSF and IL-4 for 4 days and then CNCs were added for the next 20 h. The epi-fluorescent microscopy suggested that all types of CNCs could be internalised by MoDCs (Figure 3A). However, ox-CNCs and ApA-CNCs showed a tendency for agglomeration in cell culture media, unlike nCNCs. Thereby, the agglomerated fragments of ox-CNCs and ApA-CNCs were seen in a close contact or partially surrounded by HLA-DR+ membranes of MoDCs (Supplementary Figure 2A). Semiquantitative internalisation analysis suggested that a higher proportion of MoDCs had completely internalised nCNCs, whereas oxCNCs and ApACNCs interacted with MoDCs surface as well (Supplementary Figure 2B). In line with this, nCNC-treated MoDCs displayed higher internal complexity (higher SSC parameter) after the co-cultures, whereas oxCNC- and ApACNC-treated MoDCs displayed higher FSC properties (Supplementary Figure 2C and D). These results suggested that the agglomeration and different physicochemical properties of modified CNCs lead to their lower internalization and thus they acted on MoDCs via both cell surface and intracellularly. In contrast, nCNCs were predominantly internalised by MoDCs and their intracellular amount was higher than ox- and ApA-CNCs.

Neither type of CNCs induced significant apoptosis of MoDCs after the cultures, as judged by Annexin V/7-AAD staining (Figure 3B and C). However, in contrast to nCNCs, ox-CNCs and ApA-CNCs increased the accumulation of ROS in MoDCs. Additional control in these experiments were MoDCs treated with soluble ApA at concentrations equivalent to those attached to ApA-CNCs (sApA1x) and 5 times higher concentrations (sApA5x). Soluble ApA1x did not modify apoptosis nor ROS in MoDCs, unlike sApA5x which increased ROS accumulation (Figure 3D). Ox-CNC and ApA-CNC-treated MoDCs displayed higher expression of lipidated LC3-II, in both non-starving (not shown) and starving conditions (Figure 3E), suggesting that the autophagy was also induced in MoDCs treated with modified CNCs, but not with nCNCs. Thereby, LC3-II expression was not affected by soluble ApA in either concentration tested.
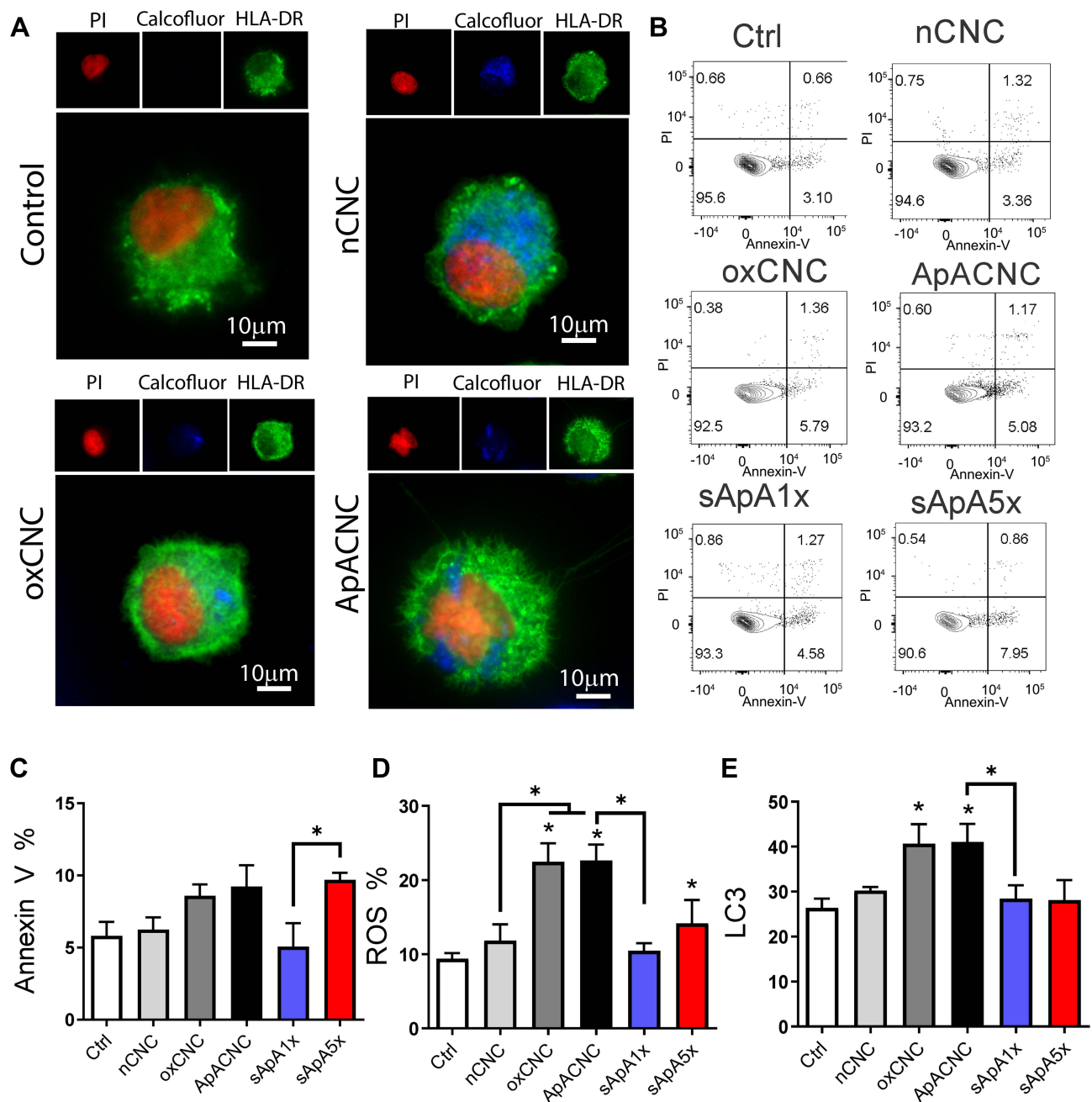
Figure 3 Interaction between CNCs and MoDCs, effects on viability, ROS and autophagy. (**A**) Epi-fluorescent microscopy images of CNC-treated MoDCs stained after the cultures with CNC by using Propidium Iodide for nuclei (red), anti-HLA-DR-Alexa Fluor 488 (green), and Calcofluor White-stained CNC (blue), see also Supplementary Figure 2. (**B**) A representative plots cell death analysis by annexin V-FITC/7-AAD staining (AnnV⁻7-AAD⁻ viable cells, AnnV⁺7-AAD⁻ early apoptotic, AnnV⁺7-AAD⁺ late apoptotic and AnnV⁻7-AAD⁺ necrotic cells) and (**C**) the summarized data showing % of total AnnV⁺ MoDCs are shown. (**D**) The proportion of ROS⁺ cells is shown, as assessed with DHE staining, and (**E**) The level of lipidated LC3-II expression is shown after 4h starvation and bafilomycin treatments of CNC-treated and control MoDCs, followed by staining of the cells with Muse Autophagy LC3-Antibody Based Kit. (**C–E**) Data are presented as mean % (or MFI for LC3-II) ± SD from three independent experiments. * $p<0.05$, compared to control, or as indicated by lines (RM-ANOVA Tukey's post-test).

Modified CNCs Induce Phenotypic Maturation of MoDCs

Considering that ROS and autophagy are critically involved in DCs functions,[41,42] we next analysed the effects of CNCs on phenotypic and functional properties of MoDCs. The maturation of MoDCs was induced with LPS/IFN-γ, a strong stimuli potentiating type 1 polarisation capacity of MoDCs.[16,22] Immature MoDCs were treated on day 4 with CNCs (200 μg/mL), 3 h hours before adding LPS/IFN-γ, for the next 16 h. Immature MoDCs displayed low expression of maturation (CD86, HLA-DR, CD83) and activation markers (NLRP3, IL-1β), and ApA-CNCs and ox-CNCs showed a weak

stimulatory effect on CD86 and HLA-DR expression, respectively. Native CNCs, in contrast, stimulated the expression of regulatory markers IDO-1 and PD1L, and reduced somewhat CD86 expression by immature MoDCs (Figure 4A and B).

LPS/IFN-γ stimuli induced the mature phenotype of MoDCs, as judged by a strong up-regulation of maturation and activation markers, but the upregulation of PD1L, ILT-3 and IDO-1 on MoDCs was detected as well (Figure 4B). Native CNC displayed mild inhibitory effects on LPS/IFN-γ-induced up-regulation of HLA-DR and NLRP3. Moreover, these nanocrystals strongly potentiated IDO-1 expression by mature MoDCs, as compared to corresponding control MoDCs. In contrast, ox-CNC-treated mature MoDCs displayed a higher expression of CD83, as compared to control, whereas other markers were not modulated significantly. The treatment of MoDCs with ApA-CNC induced the strongest MoDCs
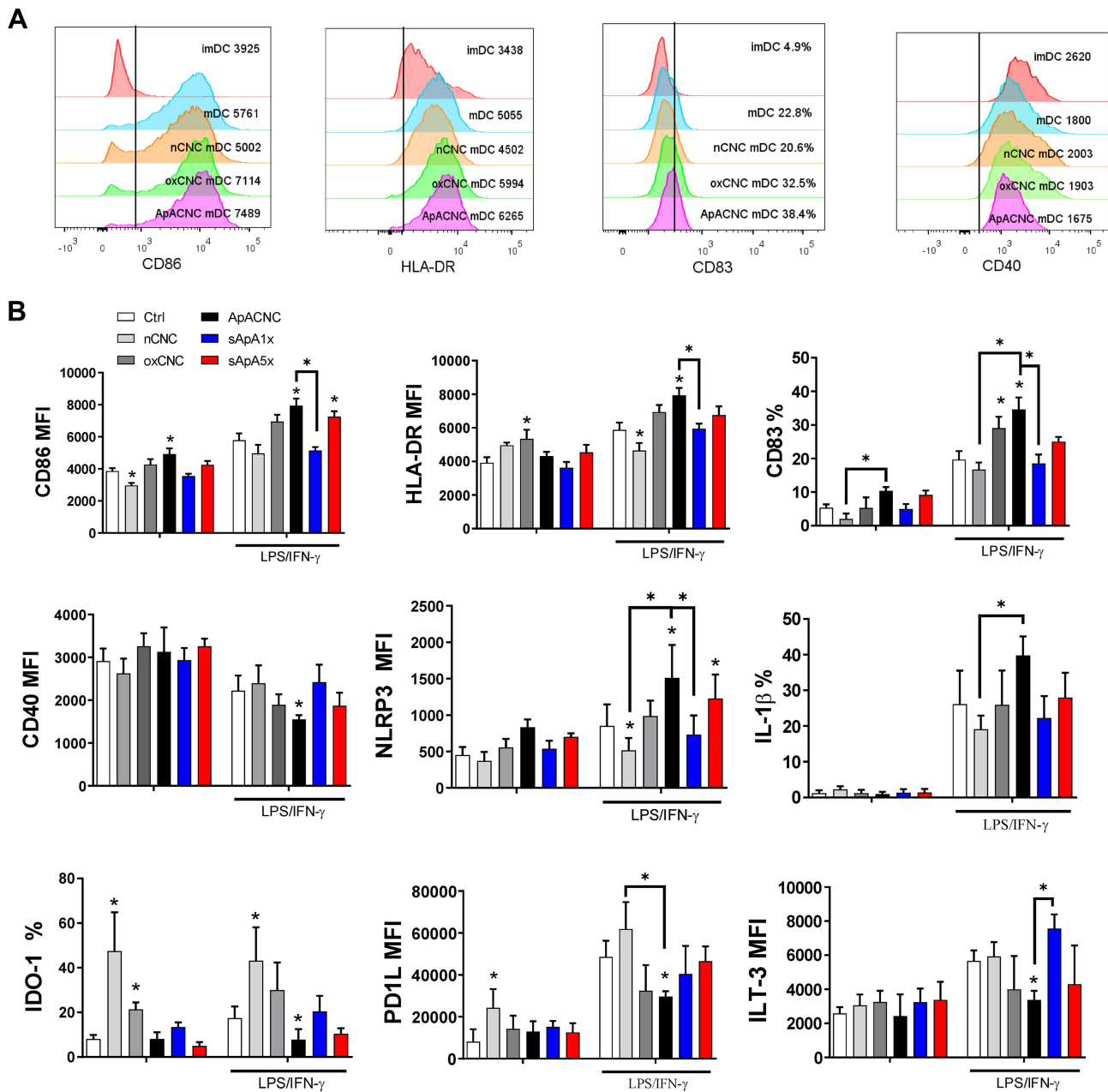

Figure 4 Effects of CNC samples on MoDCs maturation capacity. (**A**) Representative histograms of MoDCs treated on day 4 (immature (im) DCs) with CNCs (200 μg/mL), followed by stimulation with LPS/IFN-γ for the next 16h to induce mature MoDCs (mDC) are shown. (**B**) The summarized data on % or MFI (mean fluorescence intensity) of indicated markers on both immature and mature MoDCs treated with CNCs or soluble ApA (14 μg/mL, sApA1x or 70 μg/mL, sApA5x) are shown as mean ±SD of three independent experiments. * p<0.05, compared to control, or as indicated by lines (RM ANOVA, Tukey's post-test).

maturation and activation, as the expression of CD83, CD86, HLA-DR, NLRP3 and IL-1β were potentiated more than by LPS/IFN-γ alone. Additionally, PD-L1, ILT3, CD40 and IDO-1 were significantly lower on matured MoDCs pre-treated with ApA-CNC, as compared with control LPS/IFN-γ-matured MoDCs. The pro-maturing effect on MoDCs could not be achieved via soluble ApA added to a dose equivalent to that on ApACNC. However, 5 times higher dose of sApA induced a similar effect on CD86 and NLRP3 expressions by MoDCs as ApA-CNCs did, suggesting that CNCs potentiate the pro-maturing effect of ApA on MoDCs. These results indicated that CNC modified by oxidation, and ApA conjugation particularly, potentiate the phenotypic maturation and activation of MoDCs, in contrast to nCNCs which weakly affect MoDCs maturation, but potentiate the expression of tolerogenic markers by these cells.

ApA-CNCs Potentiate Allostimulatory and Th1 Polarising Capacity of MoDCs

To evaluate the functions of MoDCs treated with CNCs, we assessed their allostimulatory potential and Th polarising capacity in co-cultures with allogeneic T cells. Thereby, the allogeneic MACS-purified Cell-Trace Far Red-labelled CD3+ T cells were co-cultivated with MoDCs at different DC-to-T cell ratios for 5 days. The percentage of proliferated T cells in co-cultures with immature MoDCs, or in their absence, was weak and not modulated significantly (data not shown), whereas 20–40% of T cells proliferated in co-cultures with LPS/IFN-γ-matured MoDCs (Figure 5A). ApA-CNC-treated mature MoDCs displayed significantly increased allostimulatory capacity, and similar effects were observed with the mature MoDCs treated with sApA5x, but not sApA1x. In contrast, MoDCs treated with nCNC displayed a reduced capacity to stimulate T cell proliferation, as compared with control mature MoDCs, whereas ox-CNC-treated MoDCs did not modulate the proliferation of T cells significantly.

Some of the key cytokines involved in Th polarisation by DCs are IL-12 and IL-10.[15,43] Immature MoDCs displayed a weak to no expression of IL-12p40/p70 intracellularly (Figure 5B), and the levels of IL-12 and IL-23, which both contain p40 subunit,[15] in the culture supernatants were below the detection limit (data not shown). Mature MoDCs displayed increased expression of IL-12p40/p70, and this expression was further potentiated in MoDCs treated with ApA-CNC, but not with other CNCs or sobule ApA (Figure 5B). All CNC samples potentiated the expression of IL-10 by immature MoDCs. However, mature MoDCs treated with nCNCs and ox-CNCs expressed increased levels of IL-10 compared to the corresponding control, unlike ApA-CNC-treated mature MoDCs (Figure 5B).

In line with MoDCs cytokines, we observed a significantly higher percentage of T cells in co-cultures with ApA-CNC-treated MoDCs displaying an increased expression of IFN-γ, within both CD4+ and CD8+ T cell compartments (Figure 5C, Supplementary Figure 3). In contrast, nCNC and ox-CNC-treated mature MoDCs increased the percentage of IL-10- and IL-4-producing T cells, respectively (Figure 5C). These results suggested that the delivery of ApA via CNC potentiated its stimulatory effects on allostimulation and Th1 polarisation capacity of MoDCs. In contrast, nCNC and ox-CNC-treated MoDCs polarised the T cell's response towards increasing IL-10-producing T cells and Th2 response, respectively.

GABA-B Receptor Signalling Mediate the Effects of ApA-CNC on MoDCs Maturation, Allostimulation and Th1 Polarisation

The potentiation of allostimulatory and Th1 polarising capacity of MoDCs was observed with ApA-CNC and higher doses of soluble ApA, but not with other CNCs. Therefore, we next examined the intracellular signalling pathways by which ApA elicit these effects in MoDCs. ApA is identified as an agonist of GABA-B receptor,[44] a G-protein coupled receptor with Gαi subunits inhibiting Adenyl Cyclase activity and reducing cAMP levels.[45] First, we found that immature MoDCs express mRNA for both subunits R1 and R2 of GABA-B receptors on day 3 and 4 of differentiation, but only the R1 subunit before day 3 (Supplementary Figure 4). To investigate whether the engagement of GABA-B receptor and cAMP signalling could mediate MoDCs' functions, we treated immature MoDCs with selective GABA-B ligand baclofen, as well as with soluble ApA (1x or 5x) and ApA-CNCs, and measured cAMP levels in cell lysates after 10 minutes. The measurements showed that the basal intracellular cAMP levels were significantly reduced with baclofen treatment, as well as with sApA5x and ApA-CNCs, but not sApA1x (Figure 6A). More prominent effects were observed when MoDCs were pretreated with Forskolin, a cAMP-elevating agent,[46] suggesting that sApA5x, ApA-CNCs, like 30
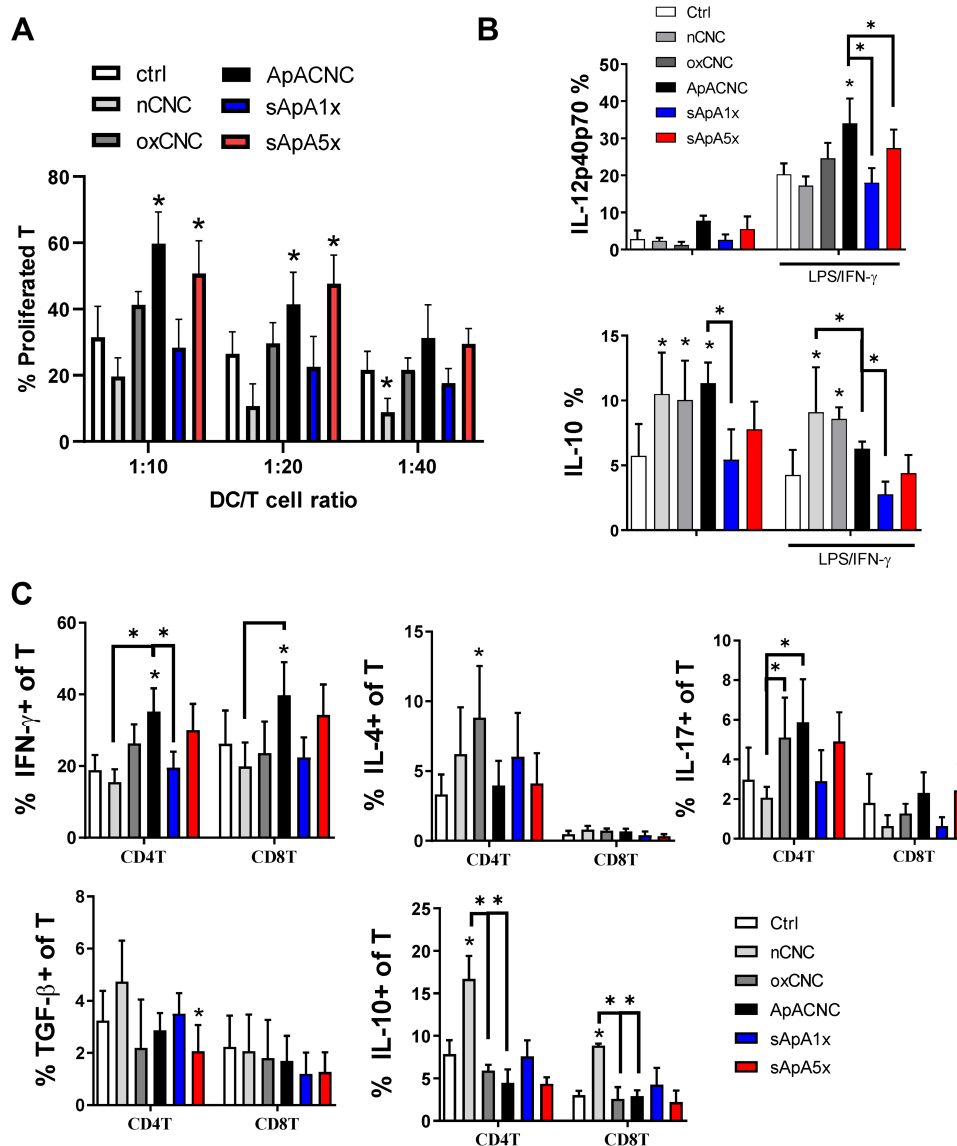
Figure 5 Effects of CNC samples on allostimulatory and Th polarising capacity of MoDCs. Immature MoDCs were treated on day 4 with CNCs (200 μg/mL), sApA1x or sApA5x, followed by stimulation with LPS/IFN-γ for the next 16h. (**A**) The proliferation of allogeneic T cells co-cultivated with LPS/IFN-γ-stimulated mature MoDCs at 1:10–1:40 DC-to-T ratio for 4 days is shown, as determined by analysing % of CellTrace Far Red ^{low}/PI$^-$ T cells by flow cytometry. (**B**) The expression of IL-12p40p70 and IL-10 in MoDCs was determined after LPS/IFN-γ stimulation, by intracellular staining on a flow cytometer. (**C**) The percentage of IFN-γ-, IL-4-, IL-17, TGF-β- and IL-10-producing CD4$^+$ and CD8$^+$ T cells were determined after 5-days of co-cultures between mature CNC-treated or control MoDCs and allogeneic T cells at 1:20 DC-to-T cell ratio (see also Supplementary Figure 3). Data is shown as mean ± SD from three (**A and B**) or four (**C**) independent experiments. * p<0.05 compared to control, or as indicated by lines (RM-ANOVA, Tukey's post-test).

μM Baclofen, reduce cAMP levels in MoDCs. The effects of baclofen, sApA5x and ApA-CNCs on the control and Forskolin-treated MoDCs were inhibited by pretreating MoDCs with a selective GABA-B Receptor inhibitor, CGP52432 (Figure 6B), suggesting that cAMP levels in MoDCs treated with ApA and ApA-CNCs were GABA-B receptor-dependent.

In addition to cAMP levels, we identified that the up-regulation of CD83, CD86 and IL-12p40/p70 by LPS/IFN-γ-stimulated MoDCs treated with ApA-CNCs was inhibited in the presence of CGP52432 (Figure 6B), as well as the capacity of MoDCs to stimulate proliferation of T cells (Figure 6C). Moreover, the ability of mature ApA-CNC-treated MoDCs to induce IFN-γ production in co-culture with allogeneic T cells was also diminished when MoDCs were pre-treated with GABA-B receptor inhibitor (Figure 6D). These data suggested that the stimulatory effects of ApA on
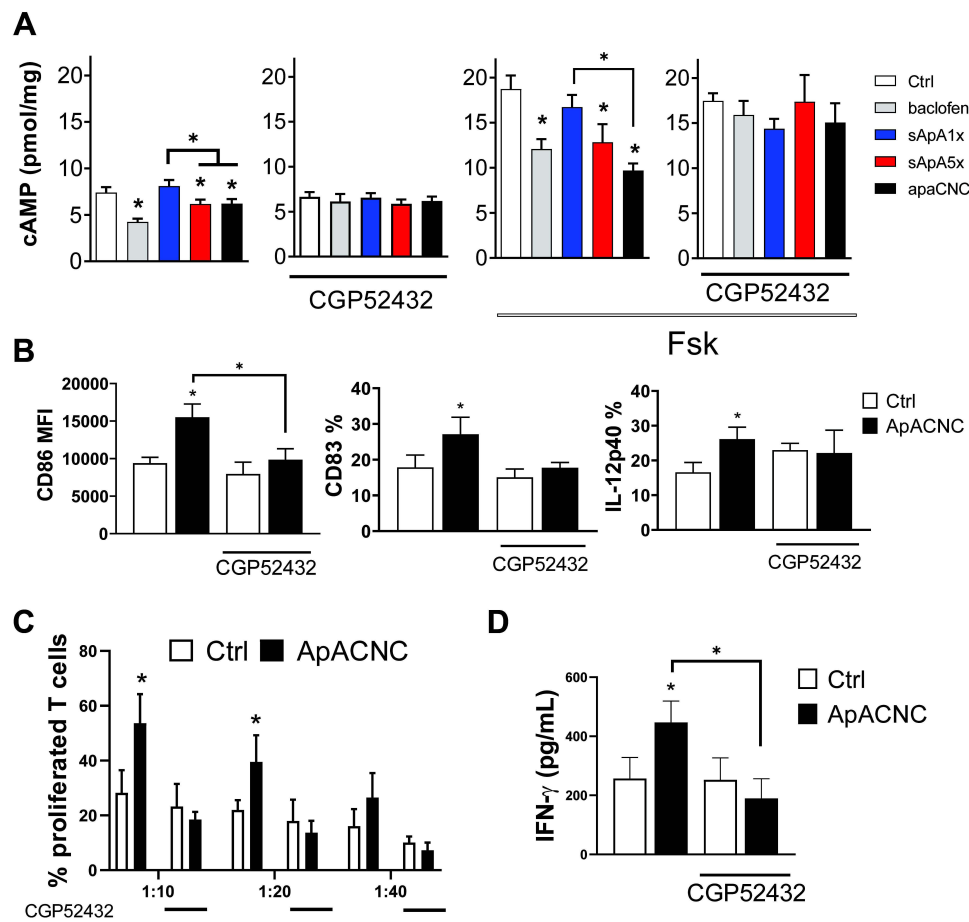
A

B

C

D

Figure 6 Role of GABA-B receptor on ApA-CNC-induced maturation of MoDCs. (**A**) cAMP levels in immature MoDCs treated with Baclofen, sApA1x, sApA5x or ApA-CNCs were determined 10 minutes after the exposure of MoDCs, in cell lysates. GABA-B Receptor inhibitor (CGP52432) was added 30 minutes before the treatments, whereas Forskolin (Fsk) was added 10 minutes before the treatments. Data on cAMP levels is shown as pmol/mg of total protein content ± SD from three independent experiments. (**B**) The levels of CD86, CD83 and IL-12p40 expression were determined on mature MoDCs, pre-treated or not with CGP52432 and ApA-CNCs. (**C**) The summarized data on the proliferation of purified T cells co-cultivated with mature MoDCs treated as in (**B**), and carried out in three DC-to-T cell ratios (1:10, 1:20 and 1:40) is shown. (**D**) The levels of IFN-γ from MoDC/T cell co-cultures are shown, as determined by ELISA from 1:20 DC/T cell co-culture supernatants. (**A–D**) The summarized data are shown as mean ± SD from three independent experiments; *p<0.05 compared to control, or as indicated by lines (RM-ANOVA Tukey's post-test).

MoDCs maturation, capacity to induce T cell proliferation and Th1 polarisation, were dependent on the GABA-B receptor/cAMP signalling pathway in MoDCs.

MoDCs Differentiated with ApA-CNCs Preserve the Immunogenic Functions When Matured with LPS/IFN-γ

Many pro-maturing agents for DCs can also inhibit their differentiation from monocytes and subsequently their immunogenic functions.[18,19] Therefore, we additionally tested how CNCs affect the differentiation of MoDCs, by treating the monocytes with the same dose of native and modified CNCs (200 μg/mL) on day 0, following 4 days of differentiation with GM-CSF and IL-4. We found that control MoDCs showed a lack of CD14 expression and a high expression of CD1a (Figure 7A and B), as expected.[22] However, when differentiated in the presence of all three types of CNCs, a significant proportion of MoDCs still expressed CD14, and the levels of CD1a expression were reduced compared to control MoDCs (Figure 7B). In addition, the expression of DC-SIGN (CD209) was significantly decreased when MoDCs were differentiated in the presence of ox-CNCs, as compared to control MoDCs. Thereby, no significant differences in % of apoptotic (Annexin-V[+]) MoDCs were observed after the differentiation of MoDCs with CNC (Figure 7C).
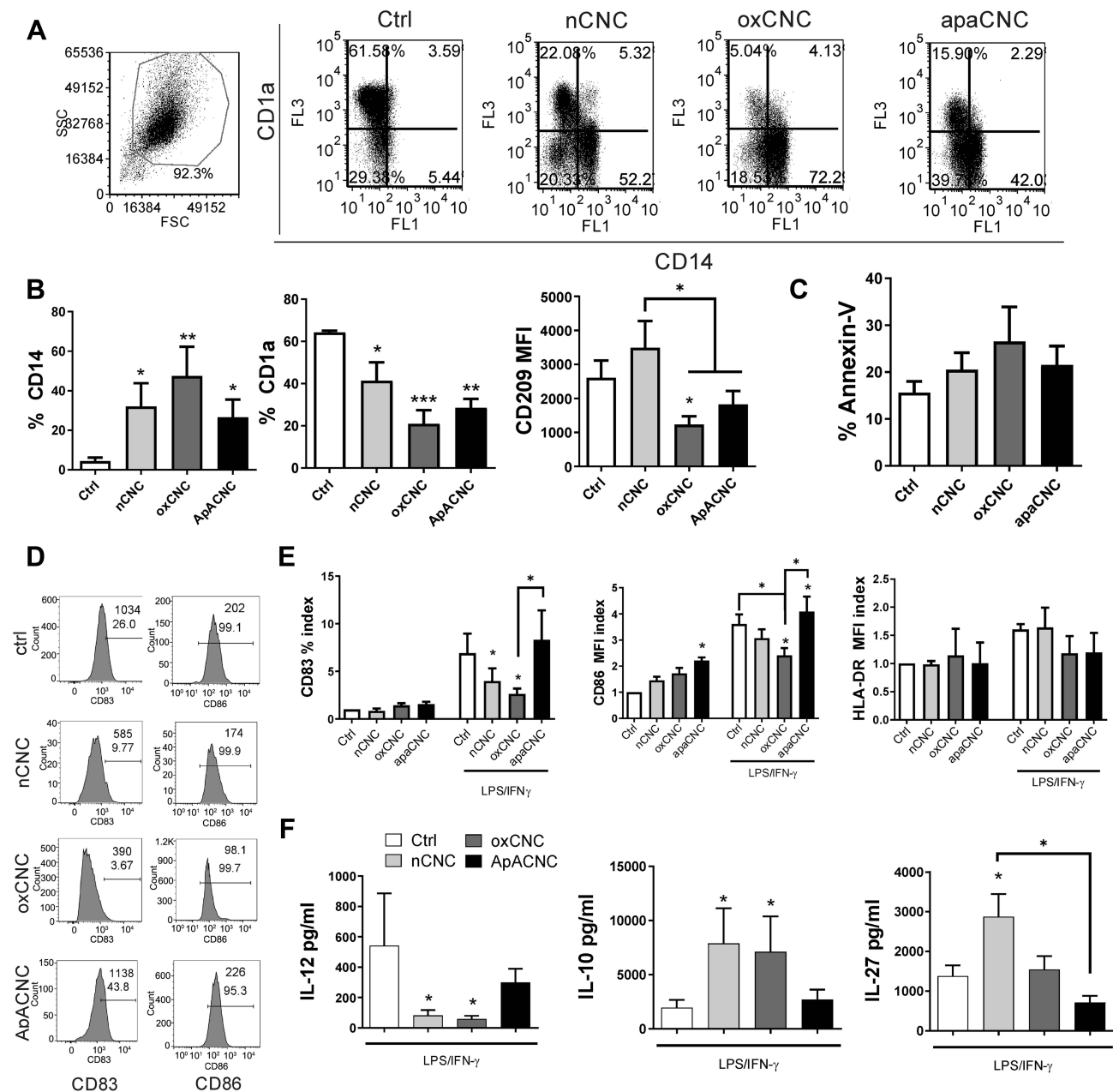
Figure 7 Effects of CNCs on MoDCs differentiation. MoDCs were differentiated with GM-CSF/IL-4, either in the presence or absence of CNC samples (200 µg/mL), for 4 days, followed by stimulation of MoDC with LPS/IFN-γ. (**A**) A representative analysis of CD1a/CD14 co-expression on MoDCs differentiated with CNC samples on day 4 is shown, and (**B**) the summarized data is shown as mean ± SD from 4 independent experiments. (**C**) The analysis of Annexin-V expressing MoDCs was carried out on day 4 of differentiation with CNC samples. (**D**) The maturation markers on MoDCs were analysed after the stimulation with LPS/IFN-γ, and the results from a representative experiment are shown with % of positive cells and MFI, and (**E**) The summarized results on CD83, CD86, HLA-DR expression are shown as fold change (index) of % (CD83) or MFI, relative to control non-treated immature MoDCs (1). (**F**) The levels of cytokines (IL-12, IL-27 and IL-10) were analysed from the supernatants of LPS/IFN-γ-stimulated MoDCs. (**C, E and F**) The data are shown as mean ± SD of three independent experiments. * $p<0.05$, **$p<0.01$, ***$p<0.05$ compared to corresponding control MoDCs (ctlr), or as indicated by lines (RM-ANOVA, Tukey's post-test).

Native CNCs and ox-CNCs did not alter the expression of CD83, CD86 and HLA-DR on immature MoDCs. In contrast, MoDCs differentiated in the presence of ApA-CNCs showed an increased expression of CD86 (Figure 7D and E). Importantly, we observed that LPS/IFN-γ stimulation of MoDCs differentiated in the presence of nCNCs and ox-CNCs induced a weaker up-regulation of CD83 and CD86, but not in ApA-CNC-differentiated MoDCs. In addition, the expression of CD86 by ApA-CNC-differentiated MoDCs increased compared with control LPS/IFN-γ-matured MoDCs (Figure 7E). The cells differentiated in the presence of nCNCs and ox-CNCs also displayed a significantly attenuated capacity to produce IL-12p70, and a higher capacity to

produce IL-10, as compared to control mature MoDCs (Figure 7F). MoDCs differentiated with nCNCs also displayed an increased capacity to produce IL-27. The production of IL-10 and IL-27 by mature ApA-CNC-differentiated MoDCs was similar to that of control mature MoDCs. IL-12p70 production by ApA-CNC-treated MoDCs was somewhat lower than that of control mature MoDCs, but not significantly. These results suggested that MoDCs differentiated in the presence of nCNCs and ox-CNCs, but not ApA-CNCs, display an impaired functional property upon maturation with LPS/IFN-γ.

MoDCs Differentiated with nCNCs and ox-CNCs, but not ApA-CNCs Display Tolerogenic Potential

Based on the phenotype and maturation potential of MoDCs-differentiated with three types of CNCs, we observed that in co-cultures with allogeneic T cells nCNC- and ox-CNC-differentiated MoDCs had a lower capacity to stimulate T cell proliferation, as compared to control. The proliferation of co-cultures with MoDCs differentiated with ApA-CNCs was higher than in control co-cultures (Figure 8A and B). Additionally, the analysis of cytokines in mature MoDCs/T cell co-cultures suggested that nCNC and ox-CNC-differentiated MoDCs potentiated the production of IL-5 and TGF-β, and downregulated IFN-γ levels in the co-cultures (Figure 8C). MoDCs differentiated with all three types of CNC displayed a diminished capacity to induce IL-17 compared to control. The Th1 polarisation capacity of ApA-CNC-differentiated mature MoDC was somewhat lower than that of control mature MoDCs, particularly on account of reduced IFN-γ production by CD4$^+$T cells (Supplementary Figure 5). However, the total levels of IFN-γ in co-cultures were higher than those observed in co-cultures with nCNC- and ox-CNC-differentiated MoDCs. These results suggested that even though ApA-CNCs altered the differentiation of MoDCs, they did not severely impair their maturation, allostimulatory and Th1 polarisation capacity.

The functions of nCNC and ox-CNC-differentiated MoDCs suggested their increased tolerogenic potential, especially since these mature MoDCs displayed an increased expression of tolerogenic markers upon maturation such as PD1L, IL-33, IDO-1 and ILT-3, as compared to control MoDCs (Supplementary Figure 6). To confirm this hypothesis, we tested the capacity of CNC-differentiated MoDCs to induce Tregs in co-cultures. It was found that immature MoDCs differentiated with nCNCs and ox-CNCs increased the percentage of CD4$^+$CD127$^-$CD25$^+$FoxP3$^+$ Tregs, as compared to control MoDCs, and nCNCs displayed such an effect even if MoDCs were additionally treated with LPS/IFN-γ (Figure 8D and E). FoxP3$^+$ Tregs produced TGF-β, IL-10, and nCNC-differentiated mature MoDCs increased the expression of both cytokines in FoxP3$^+$ Tregs (Figure 8D). In contrast, ApA-CNC-treated MoDCs did not induce significant levels of Tregs. Besides FoxP3$^+$ Tregs, we observed that nCNC-differentiated mature MoDCs also increase the percentage of CD4$^+$CD127$^-$CD25$^+$FoxP3$^-$IL-10$^+$ Tregs, which correspond to Tr-1 cells[47] (Figure 8E). Cumulatively, these results suggested that unlike ApA-CNC-differentiated MoDCs, ox-CNC- and especially nCNC-differentiated MoDCs, display an increased tolerogenic potential and the capacity to induce Tregs.

Discussion

In recent years, wood-based CNCs have attracted much attention, especially for biomedical applications, including implants, drug delivery, and tissue engineering.[3–5] CNCs can be designed to be easily resorbable and their clearance pathways modulated, by controlling their size, colloidal stability, and crystallinity via different modification methods.[3] Although the understanding of how CNCs modifications affect their cytotoxicity in vitro and in vivo is growing rapidly,[3–5] there is still a significant lack of knowledge on how CNCs affect the immune response, which is a prerequisite for their successful therapeutic application. Bisphosphonates are potent inhibitors of osteoclast-mediated bone resorption in bone-tumours,[11] and CNCs demonstrated a preference to transiently migrate into bone tissues and deliver specific drugs to these hardly accessible sites.[7,9] Previously, we showed that bisphosphonates conjugated to CNCs display good biocompatibility and a high potential for drug-delivery in human osteoblasts,[13] but the immunological properties of these nanomaterials remain unknown. Here, we compared the native, oxidised and ApA- modified CNCs, and demonstrated for the first time that nCNCs display predominantly anti-inflammatory and pro-tolerogenic properties in human immune cells. However, the oxidation and conjugation of CNCs with ApA significantly change their physical properties and convert the pro-tolerogenic properties of nCNCs into pro-inflammatory and Th1 polarising properties. Thereby, the conjugation of ApA to CNCs potentiate their capacity to increase the
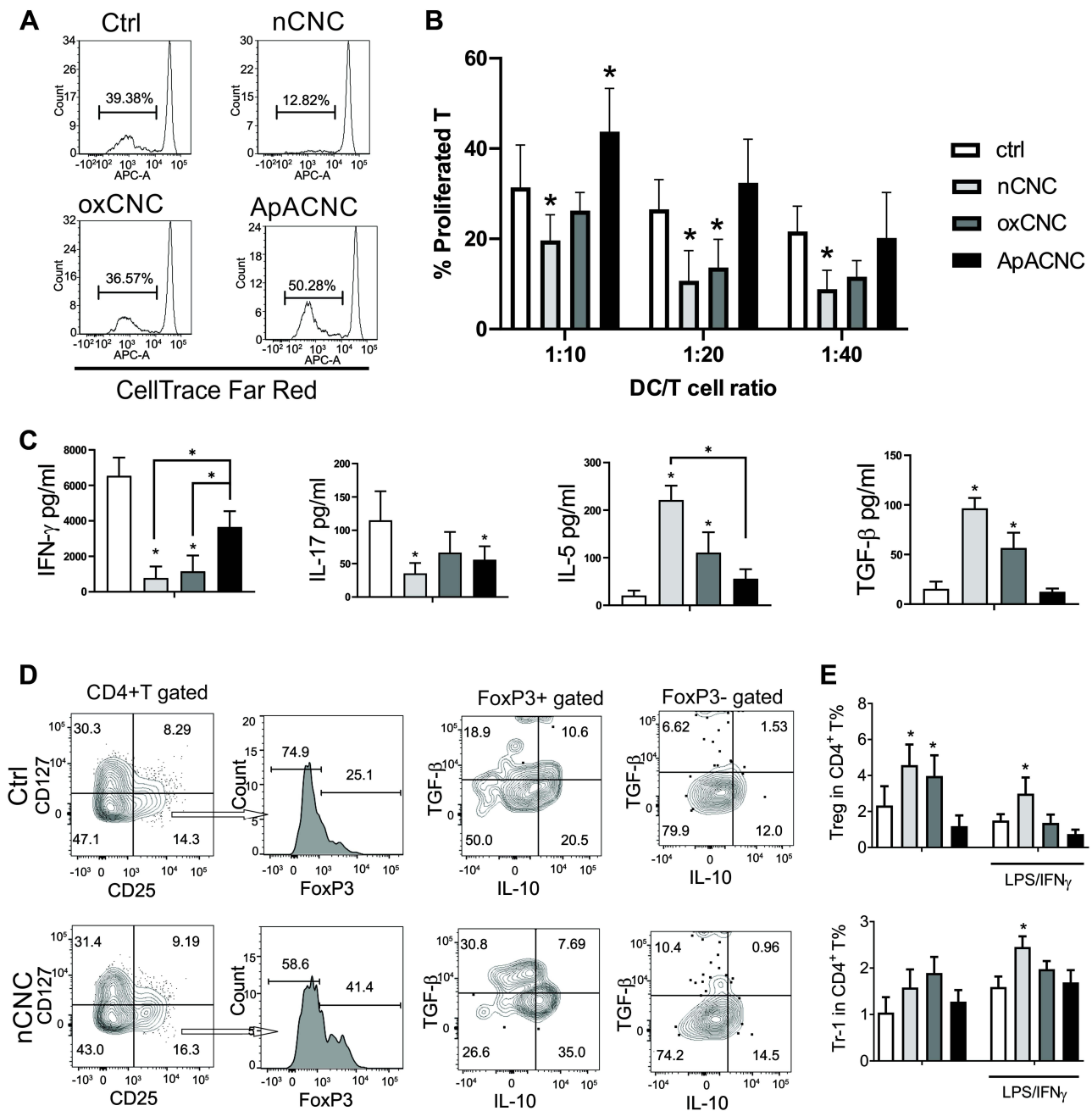
Figure 8 Allostimulatory and Th polarizing capacity of MoDCs differentiated with CNCs. MoDCs were differentiated with GM-CSF/IL-4, either in the presence or absence of CNC samples, for 4 days, followed by stimulation of MoDCs with LPS/IFN-γ. (**A**) A representative experiment on the proliferation of allogeneic T cells co-cultivated with LPS/IFN-γ-stimulated mature MoDCs that were differentiated with CNCs is shown as determined by analysing % of CellTrace Far Red[low] live T cells by flow cytometry, and (**B**) the summarized data on allogeneic proliferation in co-cultures at 1:10–1:40 DC-to-T ratio is shown, as mean ± SD of three independent experiments. (**C**) The levels of indicated cytokines were determined by ELISA in 5-day mature MoDC/T cell co-cultures at 1:20 DC-to-T cell ratio. (**D**) A representative analysis of IL-10 and TGF-β producing regulatory T cells is shown. Namely, CD25$^+$CD127$^-$ cells within CD4$^+$ T cells were gated for FoxP3 expression, and within FoxP3$^+$ and FoxP3$^-$ cells, the co-expression of IL-10 and TGF-β was analysed. (**E**) The summarised data for conventional Tregs (considered as CD4$^+$CD127$^-$CD25$^+$FoxP3$^+$) and Tr-1 cells (CD4$^+$CD127$^-$CD25$^+$FoxP3$^-$IL-10$^+$) are shown as mean ± SD of three independent experiments. * p<0.05 compared to corresponding control MoDCs, or as indicated by lines (RM-ANOVA, Tukey's post-test).

Th1 polarization potential of MoDCs via GABA-B receptors, all of which could be harnessed to improve the therapy of bone tumours significantly.

Most papers demonstrated that CNCs do not cause significant cytotoxicity in primary cells and cell lines at doses up to 300 μg/mL.[3–5] However, higher doses were shown to reduce cell viability, by upregulating the expression of stress and

apoptosis-related genes. The particular cytotoxic dose of CNCs, ranging from 300 µg/mL to 5000 µg/mL, highly depends on CNCs' source, crystallinity, size and surface modification.[3,48] In line with this, we have found that irrespective of modification, CNCs do not induce significant necrosis and apoptosis of human PBMCs at doses lower than 400 µg/mL. However, different immunomodulatory potential of CNCs was observed in PHA-stimulated PBMCs cultures, depending on the dose applied and CNCs' modification. Previous studies reported either immunostimulatory effects at sub-toxic doses, or no modulatory effects of native CNCs in vitro.[30,49,50] For example, Catalán et al[49] showed that the microcrystalline cellulose at a dose of 300 µg/mL, but not at lower doses, can induce TNF-α and IL-1β production by LPS-activated human monocyte-derived macrophages, which correlated with mild reduction of cell viability in these cultures. Similarly, Sunasee et al[50] showed that nCNCs do not alter IL-1β expression by mouse J774A macrophages and human PBMCs at 50 µg/mL after 24 h cultures, unlike cationic CNCs which potentiated the induction of ROS, secretion of ATP and IL-1β. However, up to now, it remained unknown whether any regulatory cytokines are modulated by the non-toxic doses of CNCs. For the first time, our results showed that nCNCs could induce anti-inflammatory response in PHA-stimulated PBMCs culture in non-toxic doses (100 µg/mL), according to their capacity to inhibit the proliferation of PBMCs, and down-regulate the proinflammatory cytokines production. This phenomenon was probably related to the high capacity of nCNCs to up-regulate IL-10 production by PBMCs, a cytokine with known anti-inflammatory and anti-proliferative properties.[14] Although the PHA-stimulated PBMCs model is generally good for screening the immunomodulatory potential of nanomaterials,[22,38] it cannot reveal detailed immunological mechanisms underlying the observed effects. Therefore, we further investigated the immunomodulatory potential of CNCs in human MoDCs and interaction with T lymphocytes since APCs are the most important mediators of immunomodulatory effects of nanomaterials.[51] Moreover, the immunomodulatory effects observed in the PHA-PBMCs model rely on the presence of APCs within PBMC and their interactions with lymphocytes.[39,40]

MoDCs internalised nCNCs to a higher extent than ox-CNCs and ApA-CNCs, as demonstrated by epi-fluorescent microscopy and flow cytometry. However, due to Abbe's diffraction limit and the photobleaching of calcofluor, our direct microscopy analyses were limited to the observations of larger intracellular accumulations of CNCs. The internalisation of CNCs was shown to highly depend on physico-chemical properties of CNC, such as size and surface chemistry. Our previous analyses of fluorescence-labelled nCNCs, ox- and ApA-CNCs by DLS and NTA suggested that the size of native CNCs is reduced by oxidation due to the thinning effect of periodate,[52] and the increase of ApA-CNCs thickness could be a result of the shedding of negative charges from phosphates leading to ApA-CNCs aggregation.[13] These phenomena were also observed in this work by a more precise AFM analysis. Alternative oxidation procedures for CNCs, such as TEMPO oxidation[26] or high-energy oxidation,[53] could also be applied to increase the presence of reactive aldehyde group in ox-CNCs, and therefore increase the amount of ApA conjugation to CNC surface, making them a highly versatile platform for controllable conjugation. The changes in the structure of CNCs after the oxidation and conjugation have resulted in an increase in elasticity modulus and hardness of CNCs upon modification. Different factors such as geometrical shape, structure, anisotropy and the orientation direction of individual CNCs were shown to play essential roles in forming the network in the solution casting film.[54] The measured values for the CNCs are comparable to those of other cellulose films studied. Landry et al[32] measured the modulus of the CNCs films made from softwood kraft pulp, and found that the elastic modulus and hardness of CNC films were 6.5 GPa and 0.26 GPa, respectively. Hoeger et al[55] prepared aligned ramie fiber CNC films by a convective-shear assembly system, finding that the elastic transversal modulus and hardness of CNC films were 8.3 ± 0.9 GPa and 0.38 ± 0.03 GPa, respectively. Elastic moduli between 2 and 6 GPa have been reported for CNCs prepared by sulfuric acid hydrolysis of varying hydrolysis time,[56] which is in line with our observations. The increase in elastic modulus and hardness after the oxidation and ApA-modification, shown here for the first time, could have important effects on the interaction between these nanocrystals and cells. Namely, it was demonstrated that nanoparticles with higher softness are internalised to a higher extent,[36] which is in line with the higher internalisation of nCNCs compared to ox-CNCs and ApA-CNCs. In addition, different zeta potential of native and modified CNCs could have affected their internalisation. Zeta potential between −20mV and −30mV for CNCs is considered moderately stable, whereas the potential between −10mV and −20mV causes lower stability of nanoparticles.[57] We showed previously that nCNCs at pH 7.4 PBS display a z-potential lower than −20mV, but the oxidation and ApA modification increase this potential to about −15mV in PBS.[13] This reduction in z-potential probably

caused some agglomeration of ox-CNCs and ApA-CNCs, leading to their lower internalisation and higher incidence of interaction with the cell surface. Based on different levels of internalisation, we showed previously that higher internalisation of non-conjugated, negatively charged gold[23] and graphene[22] nanoparticles correlated with their stronger tolerogenic effects on MoDCs, which is in line with the effects of nCNC. Although the exact mechanisms underlying these phenomena remain unclear, it is possible that overloaded endosomes provide specific intracellular signals leading to diminished cellular functions of MoDCs. Wang et al[30] showed previously that the accumulation of nCNC 200–300 nm induces lysosome damage, leading to ROS production and IL-1β secretion by THP-1 cells. However, nCNCs used in our study were smaller than 200 nm[13] and they did not induce ROS in MoDCs, which could explain their different modulatory effects. Other studies have shown that the accumulation of undegraded cargo inside the lysosomes is a sufficient signal to induce the translocation of STAT3 into the nucleus. STAT3 is a transcription factor leading to inhibition of DC maturation and functions, and it is directly involved in the up-regulation of IL-10 and IL-6, as well as the inhibition of Th1 polarising capacity of DCs,[58,59] although other functions for STAT3 were described as well.[60] Therefore, additional studies should be performed to better understand the role of STAT3 in nanoparticle-induced tolerance in immune cells.

Both ox-CNCs and ApA-CNCs induced ROS in MoDCs during the cultures, which correlated with their stimulatory effects of MoDCs maturation. In line with this, Wang et al[30] showed that CNCs that induce the highest ROS levels also induce the highest maturation (MHC-II, CD40, CD86, IL-1β) of mouse bone-marrow DCs. ROS are critically involved in the induction of DCs maturation, partly via activation of NF-kB,[61] but also in induction of autophagy in DCs.[22,41] Recently, Despres et al[62] showed that anionic CNCs induce ROS and ATG13 expression in LPS-stimulated macrophage cell line, but no significant changes were observed in the overall LC3-II expression, so the effects of CNCs on autophagy remained inconclusive. To the best of our knowledge, this is the first report showing that CNCs induce autophagy in MoDCs, and subsequently potentiate their maturation. The role of autophagy in DCs maturation can be either stimulatory or inhibitory.[41] Prins et al[63] found on several DC cell lines and MoDCs, that LPS-induced maturation, antigen presentation and pro-inflammatory cytokines production are impaired when the autophagy is blocked, supporting our hypothesis that ApA-CNC and ox-CNC-induced autophagy contributed to MoDCs maturation. These effects were more pronounced in MoDCs treated with LPS/IFN-γ, which induced their strong maturation.[16,22] However, LPS/IFN-γ also upregulated the expression of PD1L, IDO-1 and ILT-3, which are involved in the induction of T cell anergy and regulatory T cells.[64,65] Both LPS and IFN-γ were shown previously to up-regulate PD1L and IDO-1 expression in DCs as a negative regulatory mechanism activated during the maturation[66–69] and the similar phenomenon was observed for ILT-3 expression after LPS stimulation.[70] Importantly, the up-regulation of PD1L, ILT-3 and IDO-1 was significantly attenuated in ApA-CNC-treated mature MoDCs, which probably contributed to the unexcelled allostimulatory capacity of these cells in addition to up-regulated CD86 and HLA-DR, two key signals for T cell proliferation.[14] ApA-CNC-treated mature MoDCs also displayed the highest IL-12p40/p70 to IL-10 expression ratio, leading to their pronounced capacity to induce IFN-γ-producing CD4 and CD8 T cells, as expected.[43] PHA-PBMC model could not show the Th1 polarising potential of ApA-CNCs, most probably since the induction of Th1 cells from naïve alloreactive T cells requires more time and specific culture conditions. The downregulation of CD40 expression by ApA-CNCs could have additionally contributed to the increased Th1 polarisation by ApA-CNC-MoDCs, since CD40 is described as an essential costimulatory molecule contributing to Th2 polarisation.[71] A key mechanism that shifts the polarisation towards Th2 differentiation is IL-10-mediated inhibition of IL-12 production by DCs.[43] These well-known mechanisms could be responsible for the increased capacity of ox-CNC-treated mature MoDCs to produce both increased levels of IL-10, and subsequently induce more IL-4-producing T cells in the co-cultures. It should be noted that some of the signals detected during our intracellular measurements of IL-12p40p70 could also come from p40p19 dimer, the IL-17-polarizing cytokine IL-23,[15] although we did not find a significantly increased proportion of Th17 cells in ApA-CNC-treated MoDCs co-cultures. Irrespective of that, both Th1 and Th17 cells were shown to contribute to tumour reduction,[72,73] unlike the pro-tumorigenic Th2 cells.[74] Therefore, an increased potential of ApA-CNC-treated MoDCs to induce Th1 could be relevant for the potential application of these nanomaterials in tumour therapy, and further studies are required to confirm this hypothesis in appropriate animal models. Recently, Zoia et al[9] used CNCs modified with ALN and doxorubicin, and showed that CNCs preserve the tropism in the bone tissues, which is promising for potential osteosarcoma therapy. However, ALN conjugation to CNC increased its toxicity for Raw264.7

macrophages in vitro, and off-target conjugate accumulation to the lungs and liver.[9] Efficient targeting of DCs and potentiation of their capacity to induce Th1 and CTL immune response via nanoplatforms seems a much better strategy for cancer immunotherapy,[75] and in this context, ApA-CNCs display promising immunological properties.

Key findings in this work suggested that ApA attached to CNCs stimulates the maturation and functions of MoDCs via GABA-B-mediated reduction of cAMP levels in MoDCs. ApA has been identified as a partial agonist of GABA-B receptor[44] which signals through Gαi, and inhibits adenylyl cyclase activity.[45] Unlike the effects of GABA-A receptor ligation, leading to suppression of inflammation and leukocyte migration,[76] the immunological effects of GABA-B receptor are somewhat unclear.[77] Huang et al[78] showed that GABA-B agonist, Baclofen at 100 μM reduces the capacity of DCs to induce Th17 cells in vitro. Although the authors did not measure cAMP levels in DCs, it is also possible that higher doses of Baclofen activate adenylyl cyclase activity and cAMP levels via Gβγ protein.[45] In line with this, we observed that Baclofen at 100μM increases cAMP levels in MoDCs, whereas 30 μM baclofen decreases it (data not shown). Therefore, the levels of cAMP are probably detrimental to the regulation of MoDCs functions. Accordingly, Heystek et al[79] showed that DCs have a reduced ability to produce IL-12p70, TNF-α and polarise Th1 response upon lipopolysaccharide or CD40L stimulation in the presence of a cAMP-specific phosphodiesterase (PDE) 4 inhibitors that increase cAMP levels. These results align with our findings that ApA-CNC and soluble ApA (70 μg/mL) decrease cAMP levels and potentiate the Th1 polarizing activity of MoDCs, all of which could be blocked with a specific GABA-B inhibitor. GABA-B receptor signalling is enabled only when the R1 and R2 subunits form heterodimer.[45] By analysing the kinetics of R1 and R2 subunit mRNA expression during MoDCs differentiation, we demonstrated for the first time that the R2 subunit is expressed only after day 3 of MoDCs differentiation, but not earlier. This could explain the different functions of MoDCs differentiated with ApA-CNCs compared to MoDCs differentiated with nCNCs and ox-CNCs. Therefore, further investigations are needed to better understand the functions of GABA-B receptors in DC biology and their role in interactions with ApA-CNCs.

Agents that induce strong activation and maturation of DCs can also inhibit their differentiation if present at the early differentiation stage, which can lead to differentiation of tolerogenic DCs.[18,19] This can be a major challenge for targeting DCs in vivo in cancer therapy.[75] Therefore, we also tested the effects of CNCs on MoDCs differentiation and subsequent functions. Although ox-CNC and ApA-CNC-potentiated autophagy and ROS facilitated the maturation of MoDCs, similar mechanisms could be involved in the inhibition of MoDCs differentiation. Namely, GM-CSF/IL-4 induced differentiation and survival of MoDCs rely on mammalian target of rapamycin (mTOR) complex 1 (mTORC1) which is activated via GM-CSF receptor and phosphoinositide 3-kinase (PI3K) pathway.[80] The mTORC1 negatively regulates autophagy, but it is also a target for autophagy regulators and ROS.[81–83] In line with this, ROS-inducing drug Rotenone was shown to inhibit MoDCs differentiation, as observed by inhibited down-regulation of CD14 and up-regulation of CD1a[88], a phenotype similar to MoDCs differentiated with CNCs. Despite inhibited differentiation, the maturation of MoDCs differentiated with ApA-CNCs, but not with nCNCs and oxCNCs, was mostly unimpaired after LPS/IFN-γ stimuli, as judged by unaltered CD83, CD86 and HLA-DR expression. Moreover, the allostimulatory and Th1 polarizing functions of ApA-CNC-differentiated MoDCs were preserved as compared to control LPS/IFN-γ matured MoDCs. These results suggest that, besides ROS and autophagy, additional mechanisms are involved in the modulation of MoDCs by ApACNCs. Based on the dynamics of GABA-B receptor expression, we found that it is possible that both ApA-CNC and ox-CNC acted similarly in the first three days, towards the inhibition of MoDCs differentiation via ROS and autophagy-dependent mechanisms. However, once the GABA-B receptor became functional, ApA-CNC provided additional stimulatory signals, enabling MoDCs maturation. Cumulatively, the immunological effects of ApA-CNC conjugates could be considered beneficial for tumour therapy. In this context, a good tropism of CNCs and (bis)phosphonate-CNC conjugates for bone tissues[7,9] makes them great candidates for the treatment of bone metastasis and osteosarcoma.[9,10] Additionally, we demonstrated that the delivery of ApA via CNCs also potentiates beneficial immunomodulatory effects of ApA up to 5 times, as compared to the soluble form of ApA. These results suggest that, in potential clinical application, a smaller amount of bisphosphonates would be required if they are delivered via CNC, which is especially important when adverse clinical effects of these drugs are considered.[84] However, to prove the benefits of ApA-CNCs in the therapy of bone metastasis and osteosarcoma, further studies on appropriate in vitro and in vivo experimental models are required.

In contrast to ApA-CNCs, nCNCs and ox-CNCs displayed the potential to increase the expression of IDO-1 and IL-10 by mature MoDCs, and the effect was more pronounced when they were present during differentiation of MoDCs. The expression of these molecules could explain the inhibitory effects of ox-CNC and nCNC-treated MoDCs on proliferation of T cells and their increased capacity to induce IL-10-producing T cells and regulatory T cells. Namely, IDO-1 is shown to catabolize tryptophan, an essential amino acid required for T cell proliferation and functions.[85] Both IDO-1 and IL-10 are critically involved in the induction of regulatory T cells by MoDCs.[43,85] Additionally, MoDCs differentiated in the presence of nCNCs and oxCNCs also up-regulated ILT-3, PD1L and IL-33. ILT-3 was described as a master inducer of IL-10-producing CD8 T cells,[65] as we confirmed previously in induction of tolerogenic DCs by cellulose nanofibers.[25,26] A higher tolerogenic capacity of nCNCs could be related to its strong effect to induce IL-27. Namely, IL-27 was shown to be critically involved in the induction of Tr-1 cells,[86] and emerging data suggest that Tr-1 display stronger suppressive potential than conventional FoxP3+Tregs.[26,87] IL-33 is critically involved in Th2 polarization via ST-2 receptor on naïve T cells,[88] and the higher capacity of nCNC and ox-CNC-treated MoDCs to produce IL-33 correlates with their potential to induce Th2 cells in co-cultures. All these findings could explain the immunological mechanisms induced by nCNCs and ox-CNCs on MoDCs, but additional studies are required to delineate the contribution of each mechanism to MoDCs-mediated induction of tolerance by CNCs.

Conclusion

Cumulatively, we found that CNCs can display different immunological effects on human immune cells, depending on their surface modification, and the study model applied. For the first time, we showed that native CNCs can display anti-inflammatory and tolerogenic potential in models of PHA-stimulated PBMCs and human MoDCs, respectively. Oxidation of CNCs increases their potential to induce pro-inflammatory cytokines by PHA-stimulated PBMCs and phenotypic maturation of MoDCs, probably by activating ROS and autophagy-dependent mechanisms. However, the same mechanisms induced an impaired differentiation of MoDCs, leading to their poor maturation capacity and increased expression of tolerogenic markers. In contrast, ApA-modification of CNCs displayed stimulatory effects on the maturation of MoDCs and potentiated Th1 polarization capacity of these cells via GABA-B receptor-mediated down-regulation of cAMP in MoDCs. Importantly, this capacity of MoDCs was largely preserved when ApA-CNCs were present during differentiation of MoDCs, all of which could be relevant for designing a reliable platform for the therapy of cancer in future endeavours.

Abbreviations

7-AAD, 7-amino-actinomycin D; AFM, atomic force microscopy; ALN, alendronate; APC, Allophycocyanin; APC, antigen-presenting cells; ATR, Attenuated total reflection; ApA, 3-AminoPropylphosphonic Acid; CD, cluster of differentiation; CNC, cellulose nanocrystals; CNF, cellulose nanofibers; CTL, cytotoxic (CD8) T lymphocytes; Cy, Cyanin; DC-SIGN, Dendritic Cell-Specific Intercellular adhesion molecule, ATP, adenosine tri phosphate; DHE, dihydroethidium; DLS, Dynamic light scattering; ELISA, enzyme-linked immunosorbent assay; EPR, Enhanced Permeability and Retention; Er, reduced (elastic) modulus; FITC, fluorescein isothiocyanate; FMO, fluorescence minus one; FSC, forward scatter; FTIR, Fourier transform infrared spectroscopy; Fox, forkhead box; GABA, Gamma-aminobutyric acid; GM-CSF, granulocyte macrophages colony stimulating factor; HLA-DR, human leukocyte antigen DR; IDO, Indoleamine 2.3-Dioxygenase; IFN, interferon; IL, interleukin; ILT, Immunoglobulin-Like Transcript; LC3, Microtubule-associated protein 1A/1B-light chain 3; LPS, lipopolysaccharide; MACS, Magnetic activated cell sorting; MHC, major histocompatibility complex; MTT, 3-(4,5-dimethylthiazol-2-yl)-2,5-diphenyltetrazolium bromide; Mo-DC, monocyte-derived dendritic cells; NF-kB, nuclear factor kB; NLRP3, Nucleotide-binding oligomerization domain, Leucine rich Repeat and Pyrin domain 3; NTA, nanoparticle tracker analysis; PBMC, peripheral blood mononuclear cells; PBS, phosphate buffer saline; PCR, polymerase chain reaction; PD-L1, Programmed Death-Ligand 1; PDE, phosphodiesterase; PE, phycoerythrin; PHA, phytohemagglutinin; PI, propidium iodide; PI3K, phosphoinositide 3-kinase; PMA, Phorbol 12-myristate 13-acetate; PerCP, Peridinin-Chlorophyll-Protein; PxB, polymyxin B; RM-ANOVA, repeated-measures one-way analysis of variance; ROS, reactive oxygen species; RPMI, Roswell Park Memorial Institute; SDS, sodium dodecyl sulphate; SSC, side scatter; STAT3, Signal Transducer And Activator Of

Transcription 3; TEM, transmission electron microscopy; TGF, transforming growth factor; TLR, toll-like receptor; TNF, tumour necrosis factor; Th, T helper (CD4) cells; Tr1, type 1 regulatory T cells; Treg, regulatory T cells; cAMP, cyclic adenosine mono phosphate; mTORC1, mammalian target of rapamycin (mTOR) complex 1; n, native; ox, oxidation; sApA, soluble ApA; v, volume; wt, weight.

Acknowledgments

Disclosure

The authors report no conflicts of interest in this work.

References

1. Ning LIN, Dufresne A. Nanocellulose in biomedicine: current status and future prospect. *Eur Polym j*. 2014;59:302–325. doi:10.1016/j.eurpolymj.2014.07.025
2. Tashiro K, Kobayashi M. Theoretical evaluation of three-dimensional elastic constants of native and regenerated celluloses: role of hydrogen bonds. *Polymer*. 1991;32(8):1516–1526.
3. Čolić M, Tomić S, Bekić M. Immunological aspects of nanocellulose. *Immunol Lett*. 2020;222:80–89. doi:10.1016/j.imlet.2020.04.004
4. Kupnik K, Primožič M, Kokol V, Leitgeb M. Nanocellulose in drug delivery and antimicrobially active materials. *Polymers*. 2020;12(12):2825. doi:10.3390/polym12122825
5. Endes C, Camarero-Espinosa S, Mueller S, et al. A critical review of the current knowledge regarding the biological impact of nanocellulose. *J Nanobiotechnology*. 2016;14(1):78. doi:10.1186/s12951-016-0230-9
6. Drogat N, Granet R, Sol V, et al. Cellulose nanocrystals: a new chlorin carrier designed for photodynamic therapy: synthesis, characterization and potent anti-tumoural activity. *Photodiagnosis Photodyn Ther*. 2011;8(2):157. doi:10.1016/j.pdpdt.2011.03.114
7. Colombo L, Zoia L, Violatto MB, et al. Organ distribution and bone tropism of cellulose nanocrystals in living mice. *Biomacromolecules*. 2015;16(9):2862–2871. doi:10.1021/acs.biomac.5b00805
8. Goltzman D. Osteolysis and cancer. *J Clin Invest*. 2001;107(10):1219–1220. doi:10.1172/JCI13073
9. Zoia L, Morelli A, Talamini L, et al. Cellulose nanocrystals: a multimodal tool to enhance the targeted drug delivery against bone disorders. *Nanomedicine*. 2020;15(23):2271–2285. doi:10.2217/nnm-2020-0139
10. Demirci G, Guven MN, Altuncu S, Konca YU, Avci D, Yagci Acar H. (Bis)phosphonic acid-functionalized poly (ethyleneimine)–poly (amido amine)s for selective in vitro transfection of osteosarcoma cells. *ACS Appl Polym Mater*. 2021;3(8):3776–3787. doi:10.1021/acsapm.1c00297
11. Body JJ, Mancini I. Bisphosphonates for cancer patients: why, how, and when? *Support Care Cancer*. 2002;10(5):399–407. doi:10.1007/s005200100292
12. Jahnke W, Bold G, Marzinzik AL, et al. A general strategy for targeting drugs to bone. *Angew Chem Int Ed*. 2015;54(48):14575–14579. doi:10.1002/anie.201507064
13. Gorgieva S, Vivod V, Maver U, Gradišnik L, Dolenšek J, Kokol V. Internalization of (bis)phosphonate-modified cellulose nanocrystals by human osteoblast cells. *Cellulose*. 2017;24(10):4235–4252. doi:10.1007/s10570-017-1432-5
14. Steinman RM, Hawiger D, Nussenzweig MC. Tolerogenic dendritic cells. *Annu Rev Immunol*. 2003;21:685–711. doi:10.1146/annurev.immunol.21.120601.141040
15. Vignali DAA, Kuchroo VK. IL-12 family cytokines: immunological playmakers. *Nat Immunol*. 2012;13(8):722–728. doi:10.1038/ni.2366
16. Qu C, Brinck-Jensen NS, Zang M, Chen K. Monocyte-derived dendritic cells: targets as potent antigen-presenting cells for the design of vaccines against infectious diseases. *Int J Infect Dis*. 2014;19:1–5. doi:10.1016/j.ijid.2013.09.023
17. Čolić M, Džopalić T, Tomić S, et al. Immunomodulatory effects of carbon nanotubes functionalized with a Toll-like receptor 7 agonist on human dendritic cells. *Carbon*. 2014;67:273–287. doi:10.1016/j.carbon.2013.09.090
18. Pavlović B, Tomić S, Đokić J, et al. Fast dendritic cells matured with Poly (I:C) may acquire tolerogenic properties. *Cytotherapy*. 2015;17(12):1763–1776. doi:10.1016/j.jcyt.2015.08.001
19. Rotta G, Edwards EW, Sangaletti S, et al. Lipopolysaccharide or whole bacteria block the conversion of inflammatory monocytes into dendritic cells in vivo. *J Exp Med*. 2003;198(8):1253–1263. doi:10.1084/jem.20030335
20. Raker VK, Domogalla MP, Steinbrink K. Tolerogenic dendritic cells for regulatory t cell induction in man. *Front Immunol*. 2015;6. doi:10.3389/fimmu.2015.00569
21. Đokić J, Tomić S, Marković M, Milosavljević P, Čolić M. Mesenchymal stem cells from periapical lesions modulate differentiation and functional properties of monocyte-derived dendritic cells. *Eur J Immunol*. 2013;43(7):1862–1872. doi:10.1002/eji.201243010
22. Tomić S, Janjetović K, Mihajlović D, et al. Graphene quantum dots suppress proinflammatory T cell responses via autophagy-dependent induction of tolerogenic dendritic cells. *Biomaterials*. 2017;146:13–28. doi:10.1016/j.biomaterials.2017.08.040
23. Tomić S, Đokić J, Vasilijić S, et al. Size-dependent effects of gold nanoparticles uptake on maturation and antitumor functions of human dendritic cells in vitro. *PLoS One*. 2014;9(5):e96584. doi:10.1371/journal.pone.0096584
24. Guo J, Zhou X. Regulatory T cells turn pathogenic. *Cell Mol Immunol*. 2015;12(5):525–532. doi:10.1038/cmi.2015.12
25. Tomić S, Kokol V, Mihajlović D, Mirčić A, Čolić M. Native cellulose nanofibrills induce immune tolerance in vitro by acting on dendritic cells. *Sci Rep*. 2016;6(1):31618. doi:10.1038/srep31618

26. Tomić S, Ilić N, Kokol V, et al. Functionalization-dependent effects of cellulose nanofibrils on tolerogenic mechanisms of human dendritic cells. *Int J Nanomedicine*. 2018;13:6941. doi:10.2147/IJN.S183510

27. Shvedova AA, Kisin ER, Yanamala N, et al. Gender differences in murine pulmonary responses elicited by cellulose nanocrystals. *Part Fibre Toxicol*. 2016;13(1):28. doi:10.1186/s12989-016-0140-x

28. Yanamala N, Farcas MT, Hatfield MK, et al. In vivo evaluation of the pulmonary toxicity of cellulose nanocrystals: a renewable and sustainable nanomaterial of the future. *ACS Sustain Chem Eng*. 2014;2(7):1691–1698. doi:10.1021/sc500153k

29. Samulin Erdem J, Alswady-Hoff M, Ervik TK, Skare Ø, Ellingsen DG, Zienolddiny S. Cellulose nanocrystals modulate alveolar macrophage phenotype and phagocytic function. *Biomaterials*. 2019;203:31–42. doi:10.1016/j.biomaterials.2019.02.025

30. Wang X, Chang CH, Jiang J, et al. The crystallinity and aspect ratio of cellulose nanomaterials determine their pro-inflammatory and immune adjuvant effects in vitro and in vivo. *Small*. 2019;15(42):1901642. doi:10.1002/smll.201901642

31. Oliver WC, Pharr GM. Measurement of hardness and elastic modulus by instrumented indentation: advances in understanding and refinements to methodology. *J Mater Res*. 2004;19(1):3. doi:10.1557/jmr.2004.19.1.3

32. Landry V, Alemdar A, Blanchet P. Nanocrystalline cellulose: morphological, physical, and mechanical properties. *For Prod J*. 2011;61(2):104–112. doi:10.13073/0015-7473-61.2.104

33. Grkovic M, Stojanovic DB, Pavlovic VB, Rajilic-Stojanovic M, Bjelovic M, Uskokovic PS. Improvement of mechanical properties and antibacterial activity of crosslinked electrospun chitosan/poly (ethylene oxide) nanofibers. *Engineering*. 2017;121:58–67. doi:10.1016/j.compositesb.2017.03.024

34. Njoroge JM, Yourick JJ, Principato MA. A flow cytometric analysis of macrophage– nanoparticle interactions in vitro: induction of altered Toll-like receptor expression. *Int J Nanomedicine*. 2018;13:8365–8378. doi:10.2147/IJN.S174184

35. Ma N, Ma C, Li C, et al. Influence of nanoparticle shape, size, and surface functionalization on cellular uptake. *J Nanosci Nanotechnol*. 2013;13(10):6485–6498. doi:10.1166/jnn.2013.7525

36. Guo P, Liu D, Subramanyam K, et al. Nanoparticle elasticity directs tumor uptake. *Nat Commun*. 2018;9(1):130. doi:10.1038/s41467-017-02588-9

37. Yong MK, Cameron PU, Slavin MA, et al.. Low T-cell responses to mitogen stimulation predicts poor survival in recipients of allogeneic hematopoietic stem cell transplantation. *Front Immunol*. 2017;8. doi:10.3389/fimmu.2017.01506

38. Čolić M, Mihajlović D, Mathew A, Naseri N, Kokol V. Cytocompatibility and immunomodulatory properties of wood based nanofibrillated cellulose. *Cellulose*. 2015;22(1):763–778. doi:10.1007/s10570-014-0524-8

39. Sansom DM, Wilson A, Boshell M, Lewis J, Hall ND. B7/CD28 but not LFA-3/CD2 interactions can provide "third-party" co-stimulation for human T-cell activation. *Immunology*. 1993;80(2):242–247.

40. Antic Stankovic J, Vucevic D, Majstorovic I, Vasilijic S, Colic M. The role of rat Crry, a complement regulatory protein, in proliferation of thymocytes. *Life Sci*. 2004;75(25):3053–3062. doi:10.1016/j.lfs.2004.06.007

41. Ghislat G, Lawrence T. Autophagy in dendritic cells. *Cell Mol Immunol*. 2018;15(11):944–952. doi:10.1038/cmi.2018.2

42. Del Prete A, Zaccagnino P, Di Paola M, et al. Role of mitochondria and reactive oxygen species in dendritic cell differentiation and functions. *Free Radic Biol Med*. 2008;44(7):1443–1451. doi:10.1016/j.freeradbiomed.2007.12.037

43. Ng THS, Britton G, Hill E, Verhagen J, Burton B, Wraith D. Regulation of adaptive immunity; the role of interleukin-10. *Front Immunol*. 2013;4. doi:10.3389/fimmu.2013.00129

44. Hills JM, Dingsdale RA, Parsons ME, Dolle RE, Howson W. 3-Aminopropylphosphinic acid–a potent, selective GABAB receptor agonist in the Guinea-pig ileum and rat anococcygeus muscle. *Br J Pharmacol*. 1989;97(4):1292–1296. doi:10.1111/j.1476-5381.1989.tb12591.x

45. Black JB, Premont RT, Daaka Y. Feedback regulation of G protein-coupled receptor signaling by GRKs and arrestins. *Semin Cell Dev Biol*. 2016;50:95–104. doi:10.1016/j.semcdb.2015.12.015

46. Zanassi P, Paolillo M, Feliciello A, Avvedimento EV, Gallo V, Schinelli S. cAMP-dependent protein kinase induces cAMP-response element-binding protein phosphorylation via an intracellular calcium release/erk-dependent pathway in striatal neurons *. *J Biol Chem*. 2001;276(15):11487–11495. doi:10.1074/jbc.M007631200

47. Zeng H, Zhang R, Jin B, Chen L. Type 1 regulatory T cells: a new mechanism of peripheral immune tolerance. *Cell Mol Immunol*. 2015;12(5):566–571. doi:10.1038/cmi.2015.44

48. Tuerxun D, Pulingam T, Nordin NI, et al. Synthesis, characterization and cytotoxicity studies of nanocrystalline cellulose from the production waste of rubber-wood and kenaf-bast fibers. *Eur Polym J*. 2019;116:352–360. doi:10.1016/j.eurpolymj.2019.04.021

49. Catalán J, Ilves M, Järventaus H, et al. Genotoxic and immunotoxic effects of cellulose nanocrystals in vitro. *Environ Mol Mutagen*. 2015;56(2):171–182. doi:10.1002/em.21913

50. Sunasee R, Araoye E, Pyram D, Hemraz UD, Boluk Y, Ckless K. Cellulose nanocrystal cationic derivative induces NLRP3 inflammasome-dependent IL-1β secretion associated with mitochondrial ROS production. *Biochem Biophys Rep*. 2015;4:1–9. doi:10.1016/j.bbrep.2015.08.008

51. Ray P, Haideri N, Haque I, et al. The impact of nanoparticles on the immune system: a gray zone of nanomedicine. *J Immunol Sci*. 2021;5(1):19–33. doi:10.29245/2578-3009/2021/1.1206

52. Conley K, Godbout L, Whitehead MA, van de Ven TGM. Origin of the twist of cellulosic materials. *Carbohydr Polym*. 2016;135:285–299. doi:10.1016/j.carbpol.2015.08.029

53. Zhang R, Liu Y. High energy oxidation and organosolv solubilization for high yield isolation of cellulose nanocrystals (CNC) from eucalyptus hardwood. *Sci Rep*. 2018;8(1):16505. doi:10.1038/s41598-018-34667-2

54. Wu Q, Meng Y, Concha K, et al. Influence of temperature and humidity on nano-mechanical properties of cellulose nanocrystal films made from switchgrass and cotton. *Ind Crops Prod*. 2013;48:28–35. doi:10.1016/j.indcrop.2013.03.032

55. Hoeger I, Rojas OJ, Efimenko K, Velev OD, Kelley SS. Ultrathin film coatings of aligned cellulose nanocrystals from a convective-shear assembly system and their surface mechanical properties. *Soft Matter*. 2011;7(5):1957–1967. doi:10.1039/C0SM01113D

56. Krishnamachari P, Hashaikeh R, Chiesa M, Gad El Rab KRM. Effects of acid hydrolysis time on cellulose nanocrystals properties: nanoindentation and thermogravimetric studies. *Cellul Chem Technol*. 2012;46(1–2):13–18.

57. Bhattacharjee S. DLS and zeta potential – what they are and what they are not? *J Control Release*. 2016;235:337–351. doi:10.1016/j.jconrel.2016.06.017

58. Bauer K, Binder S, Klein C, Simon J, Horn F. Inhibition of dendritic cell maturation and activation is mediated by STAT3. *Cell Commun Signal*. 2009;7(1):A68. doi:10.1186/1478-811X-7-S1-A68

59. Melillo JA, Song L, Bhagat G, et al. Dendritic cell (DC)-specific targeting reveals Stat3 as a negative regulator of DC function. *J Immunol*. 2010;184(5):2638–2645. doi:10.4049/jimmunol.0902960

60. Hillmer EJ, Zhang H, Li HS, Watowich SS. STAT3 signaling in immunity. *Cytokine Growth Factor Rev*. 2016;31:1–15. doi:10.1016/j.cytogfr.2016.05.001

61. Cheong TC, Shin EP, Kwon EK, et al. Functional manipulation of dendritic cells by photoswitchable generation of intracellular reactive oxygen species. *ACS Chem Biol*. 2015;10(3):757–765. doi:10.1021/cb5009124

62. Despres HW, Sabra A, Anderson P, et al. Mechanisms of the immune response cause by cationic and anionic surface functionalized cellulose nanocrystals using cell-based assays. *Toxicol* In Vitro. 2019;55:124–133. doi:10.1016/j.tiv.2018.12.009

63. Prins MMC, van Roest M, Vermeulen JLM, et al. Applicability of different cell line-derived dendritic cell-like cells in autophagy research. *J Immunol Methods*. 2021;497:113106. doi:10.1016/j.jim.2021.113106

64. Qin W, Hu L, Zhang X, et al.. The *diverse functio*n of PD-1/PD-L pathway beyond cancer. *Front Immunol*. 2019;10. doi:10.3389/fimmu.2019.02298

65. Vlad G, Cortesini R, Suciu-Foca N. CD8+ T suppressor cells and the ILT3 master switch. *Hum Immunol*. 2008;69(11):681–686. doi:10.1016/j.humimm.2008.08.286

66. Forteza MJ, Polyzos KA, Baumgartner R, et al.. Activation of the regulatory T-cell/indoleamine 2,3-dioxygenase axis reduces vascular inflammation and atherosclerosis in hyperlipidemic mice. *Front Immunol*. 2018;9. doi:10.3389/fimmu.2018.00950

67. Bazhin AV, von Ahn K, Fritz J, Werner J, Karakhanova S. Interferon-α up-regulates the expression of PD-L1 molecules on immune cells through STAT3 and p38 signaling. *Front Immunol*. 2018;9. doi:10.3389/fimmu.2018.02129

68. Salazar F, Awuah D, Negm OH, Shakib F, Ghaemmaghami AM. The role of indoleamine 2,3-dioxygenase-aryl hydrocarbon receptor pathway in the TLR4-induced tolerogenic phenotype in human DCs. *Sci Rep*. 2017;7(1):43337. doi:10.1038/srep43337

69. Li Q, Harden JL, Anderson CD, Egilmez NK. Tolerogenic phenotype of IFN-γ-induced IDO+ dendritic cells is maintained via an autocrine IDO-kynurenine/AhR-IDO loop. *J Immunol*. 2016;197(3):962–970. doi:10.4049/jimmunol.1502615

70. Penna G, Roncari A, Amuchastegui S, et al. Expression of the inhibitory receptor ILT3 on dendritic cells is dispensable for induction of CD4+Foxp3+ regulatory T cells by 1,25-dihydroxyvitamin D3. *Blood*. 2005;106(10):3490–3497. doi:10.1182/blood-2005-05-2044

71. MacDonald AS, Straw AD, Dalton NM, Pearce EJ. Cutting edge: th2 response induction by dendritic cells: a role for CD40. *J Immunol*. 2002;168(2):537–540. doi:10.4049/jimmunol.168.2.537

72. Asadzadeh Z, Mohammadi H, Safarzadeh E, et al. The paradox of Th17 cell functions in tumor immunity. *Cell Immunol*. 2017;322:15–25. doi:10.1016/j.cellimm.2017.10.015

73. Aue G, Sun C, Liu D, et al. Activation of Th1 immunity within the tumor microenvironment is associated with clinical response to lenalidomide in chronic lymphocytic leukemia. *J Immunol*. 2018;201(7):1967–1974. doi:10.4049/jimmunol.1800570

74. Lee HL, Jang JW, Lee SW, et al. Inflammatory cytokines and change of Th1/Th2 balance as prognostic indicators for hepatocellular carcinoma in patients treated with transarterial chemoembolization. *Sci Rep*. 2019;9(1):3260. doi:10.1038/s41598-019-40078-8

75. Yang M, Li J, Gu P, Fan X. The application of nanoparticles in cancer immunotherapy: targeting tumor microenvironment. *Bioact Mater*. 2021;6(7):1973–1987. doi:10.1016/j.bioactmat.2020.12.010

76. Bhandage AK, Barragan A. GABAergic signaling by cells of the immune system: more the rule than the exception. *Cell Mol Life Sci*. 2021;78(15):5667–5679. doi:10.1007/s00018-021-03881-z

77. Crowley T, Fitzpatrick JM, Kuijper T, et al.. Modulation of TLR3/TLR4 inflammatory signaling by the GABAB receptor agonist baclofen in glia and immune cells: relevance to therapeutic effects in multiple sclerosis. *Front Cell Neurosci*. 2015;9. doi:10.3389/fncel.2015.00284

78. Huang S, Mao J, Wei B, Pei G. The anti-spasticity drug baclofen alleviates collagen-induced arthritis and regulates dendritic cells. *J Cell Physiol*. 2015;230(7):1438–1447. doi:10.1002/jcp.24884

79. Heystek HC, Thierry A, Soulard P, Moulon C. Phosphodiesterase 4 inhibitors reduce human dendritic cell inflammatory cytokine production and Th1-polarizing capacity. *Int Immunol*. 2003;15(7):827–835. doi:10.1093/intimm/dxg079

80. Woltman AM, van der Kooij SW, Coffer PJ, Offringa R, Daha MR, van Kooten C. Rapamycin specifically interferes with GM-CSF signaling in human dendritic cells, leading to apoptosis via increased p27KIP1 expression. *Blood*. 2003;101(4):1439–1445. doi:10.1182/blood-2002-06-1688

81. Chen CC, Jeon SM, Bhaskar PT, et al. FoxOs Inhibit mTORC1 and activate akt by inducing the expression of sestrin3 and rictor. *Dev Cell*. 2010;18(4):592–604. doi:10.1016/j.devcel.2010.03.008

82. Li M, Zhao L, Liu J, et al. Multi-mechanisms are involved in reactive oxygen species regulation of mTORC1 signaling. *Cell Signal*. 2010;22(10):1469–1476. doi:10.1016/j.cellsig.2010.05.015

83. Deleyto-Seldas N, Efeyan A. The mTOR–autophagy axis and the control of metabolism. *Front Cell Dev Biol*. 2021;9. doi:10.3389/fcell.2021.655731

84. Kennel KA, Drake MT. Adverse effects of bisphosphonates: implications for osteoporosis management. *Mayo Clin Proc*. 2009;84(7):632–638. doi:10.1016/S0025-6196(11)60752-0

85. Endo R, Nakamura T, Kawakami K, Sato Y, Harashima H. The silencing of indoleamine 2,3-dioxygenase 1 (IDO1) in dendritic cells by siRNA-loaded lipid nanoparticles enhances cell-based cancer immunotherapy. *Sci Rep*. 2019;9(1):11335. doi:10.1038/s41598-019-47799-w

86. Pot C, Apetoh L, Awasthi A, Kuchroo VK. Induction of regulatory Tr1 cells and inhibition of T(H)17 cells by IL-27. *Semin Immunol*. 2011;23(6):438–445. doi:10.1016/j.smim.2011.08.003

87. Yao Y, Vent-Schmidt J, McGeough MD, et al. Tr1 cells, but not foxp3+ regulatory T cells, suppress NLRP3 inflammasome activation via an IL-10–dependent mechanism. *J Immunol*. 2015;195(2):488–497. doi:10.4049/jimmunol.1403225

88. Zhou Z, Yan F, Liu O. Interleukin (IL)-33: an orchestrator of immunity from host defence to tissue homeostasis. *Clin Transl Immunol*. 2020;9(6):e1146. doi:10.1002/cti2.1146